Electrical Power and Energy Systems 155 (2024) 109650

Contents lists available at ScienceDirect

International Journal of Electrical Power and Energy Systems

journal homepage: www.elsevier.com/locate/ijepes

Optimal scheduling of a microgrid with power quality constraints based on demand side management under grid-connected and islanding operations

Firmansyah Nur Budiman [a,*], Makbul A.M. Ramli [a,b], Houssem R.E.H. Bouchekara [c], Ahmad H. Milyani [a,b]

[a] Department of Electrical and Computer Engineering, King Abdulaziz University, Jeddah 21589, Saudi Arabia
[b] Center of Research Excellence in Renewable Energy and Power Systems, King Abdulaziz University, Jeddah 21589, Saudi Arabia
[c] Department of Electrical Engineering, University of Hafr Al Batin, Hafr Al Batin 31991, Saudi Arabia

ARTICLE INFO

Keywords:
Optimal harmonic power flow
Microgrid scheduling
Grid-connected microgrid
Islanded microgrid
Power quality
Demand side management

ABSTRACT

Power quality (PQ) issues are direct consequences of integrating power electronics components and non-linear loads into microgrids. These issues can also be triggered by an unbalanced loading in the microgrid. Certainly, they affect the daily operation scheduling of the microgrid. This paper proposes an optimal harmonic power flow (OHPF) framework for the daily optimal scheduling of a grid-connected microgrid, which is constructed by combining the optimization formulation and harmonic power flow (HPF). Within the framework, PQ is evaluated by observing three indices including voltage magnitude, voltage total harmonic distortion (THD_V), and voltage unbalance factor (VUF). A non-iterative mitigation scheme based on demand side management (DSM) is proposed to avoid PQ indices violations and is integrated into the optimization formulation part of the OHPF as a set of load constraints. The proposed constraints allow a flexible combination of different DSM actions including load shedding and interphase load transfer (ILT). Furthermore, the constraints to limit voltage magnitude, voltage THD, and VUF are integrated into the formulation in the form of penalty functions. The software implementation of the proposed OHPF involves Julia-based JuMP.jl and Gurobi solver for optimization part and OpenDSS for harmonic load flow part. The effectiveness of the proposed framework is tested using a modified IEEE 37-bus feeder for different load fluctuations, which allow different combinations of PQ indices violations. The assessment involves both normal and intentional islanding conditions. The results demonstrate that, under different random events, the proposed framework can avoid the violation of PQ indices limits in most cases without adding an excessive computational burden to the original optimization and harmonic load flow algorithms.

1. Introduction

1.1. Background

Research works related to the microgrid are among the great interests nowadays. They cover a wide range of topics, spanning from material science, which is related to energy storage technology, to different engineering areas. In terms of the microgrid operation, the fields of optimization and control engineering are two major subjects that play important roles for the efficient operation of the microgrid, especially when it is connected to the main grid. The optimization is mainly related to the operation scheduling of the microgrid. A large number of papers related to this field have been published [1,2].

During its operation, a microgrid may be subject to a number of disturbances leading to different power quality (PQ) issues. Microgrids increasingly use renewable energy to generate their own energy. Along with other components such as the battery energy storage system (BESS), microgrids employ power electronics converter system for power conditioning. These power electronics devices are the sources of harmonics in the system. This is also aggravated by the presence of non-linear load in the system [3]. Meanwhile, the microgrids are likely to face a very fluctuating load demand which can make the voltage magnitude at the load buses either lower or higher than the permissible limits, typically 0.95 pu (lower limit) and 1.05 pu (upper limit). Another potential cause of PQ issues, in case of three-phase microgrid, is the unbalanced loading, which may trigger the voltage unbalance. All of

* Corresponding author.
E-mail address: fnbudiman@gmail.com (F.N. Budiman).

https://doi.org/10.1016/j.ijepes.2023.109650
Received 26 March 2023; Received in revised form 22 October 2023; Accepted 5 November 2023
Available online 8 November 2023

Nomenclature

Subscripts

f	Phase in a load bus; $f \in \{AB, BC, CA\}$ in case of delta connection
i	Dispatchable unit number; $i = 1, 2, \ldots, N$
k	EV number; $k = 1, 2, \ldots, K$
l	Load bus (can be linear, lighting, ASD, or other) number; $l = 1, 2, \ldots, L$

Inline Index

t	Discrete time (hour); $t = 1, 2, \ldots, T$

Constants

η_{B} & η_{EV}	Charging/discharging efficiencies of BESS and EV battery
$C_{\mathrm{B}}^{\mathrm{deg}}$	BESS degradation cost per unit energy ($/kWh)
$C_{\mathrm{EV}}^{\mathrm{deg}}$	EV battery degradation cost per unit energy ($/kWh)
$C_{\mathrm{grid}}^{\mathrm{in}}$ & $C_{\mathrm{grid}}^{\mathrm{out}}$	Market prices for energy imported from and exported to the grid ($/kWh)
C_i^{op}	Production cost of dispatchable unit i ($/kWh)
$C_{\mathrm{B}}^{\mathrm{res}}$	Value of BESS residual energy ($/kWh)
C_i^{st}	Startup cost of dispatchable unit i ($/h)
C_{μ}^{Q}	Penalty cost for reactive power exchange among microgrid components per unit energy ($/kVARh)
C_{grid}^{Q}	Penalty cost for reactive power exchange with the grid per unit energy ($/kVARh)
C_l^{LS}	Cost of shedding load/demand at bus l ($/kWh)
K	Number of EVs involved in the scheduling; $K = 30$
L	Number of load buses in the system (different load types in the same bus are deemed as different buses)
$P^{\max}$ & $Q^{\max}$	Maximum active and reactive power capability of the microgrid component (kW and kVAR)
$P_{\mathrm{grid}}^{\max}$ & $Q_{\mathrm{grid}}^{\max}$	Maximum power transfer capability with the grid (kW and kVAR)
$P_{l,f}$	Scheduled demand in phase f of load bus l (kW)
PF	Power factor of the microgrid component
$SOE^{\max}$	Maximum state of energy (kWh)
$SOE^{\min}$	Minimum state of energy (kWh)
T	Final hour of the scheduling; $T = 24$
$T_{\mathrm{EV}}^{\mathrm{arr}}$	Time (hour) at which EV arrives at charging station
$T_{\mathrm{EV}}^{\mathrm{dep}}$	Time (hour) at which EV departs from charging station

Variables

$p_{\mathrm{B}}^{\mathrm{ch}}$ & $p_{\mathrm{B}}^{\mathrm{dch}}$	Active power charged to and discharged by BESS (kW)
$p_{\mathrm{EV}}^{\mathrm{ch}}$ & $p_{\mathrm{EV}}^{\mathrm{dch}}$	Active power charged to and discharged by EV battery (kW)
$p_{\mathrm{grid}}^{\mathrm{in}}$ & $q_{\mathrm{grid}}^{\mathrm{in}}$	Active and reactive power imported from the grid (kW and kVAR)
$p_{\mathrm{grid}}^{\mathrm{out}}$ & $q_{\mathrm{grid}}^{\mathrm{out}}$	Active and reactive power exported to the grid (kW and kVAR)
p_i	Active power generated by dispatchable unit i (kW)
$p_{l,f}$ & $q_{l,f}$	Actual active and reactive power supplied to phase f of load bus l (kW and kVAR)
q^{gen} & q^{abs}	Reactive power generated and absorbed by the microgrid component (kVAR)
s	Binary variable determining the operation mode of the microgrid (0 = grid-connected; 1 = stand alone)
soe_{B} & soe_{EV}	State of energy of BESS and EV battery (kWh)
$u_{\mathrm{B}}^{\mathrm{ch}}$ & $u_{\mathrm{B}}^{\mathrm{dch}}$	Charging and discharging status of BESS (binary)
$u_{\mathrm{EV}}^{\mathrm{ch}}$ & $u_{\mathrm{EV}}^{\mathrm{dch}}$	Charging and discharging status of EV (binary)
u_i	On/off status of dispatchable unit i (1 = unit on; 0 = unit off)
v_i	Startup status of dispatchable unit i (1 = unit startup; 0 = otherwise)
w_i	Shutdown status of dispatchable unit i (1 = unit shutdown; 0 = otherwise)

Abbreviations

ASD	Adjustable speed drive
DE	Diesel engine
DG	Distributed generation
DSM	Demand side management
EV	Electric vehicle
HPF	Harmonic power flow
ILT	Interphase load transfer
MILP	Mixed integer linear programming
OHPF	Optimal harmonic power flow
PQ	Power quality
PV	Solar photovoltaic
SSM	Supply side management
STF	Single-tuned filter
THD	Total harmonics distortion
VUF	Voltage unbalance factor
WT	Wind turbine

these potential PQ problems must be considered when managing the microgrid operation scheduling [4,5].

1.2. Literature review

A number of research works on the microgrid considering PQ issues have been reported [6,7]. Based on these literature, PQ problems can be mitigated using several approaches, which are classified into two categories, including the installation of additional equipment and the enforcement of the optimization and/or control processes of the available resources in the system. The first category can be in the form of harmonic passive filter optimal design [8] and optimal allocation [9], optimal design of DSTATCOM to control reactive power flow [10], optimal design of virtual admittance and impedance [11] or virtual impedance only [12], and optimal design of DSTATCOM with optimally-tuned PID controller [13]. In [14], a virtual-impedance-based technique is also used. A cost-function-based method for the improvement is proposed, which is further optimized by using continuous-control-set model predictive control (MPC). In addition to passive filter, active filter is also used [15]. In case of temporary PQ problems, however, this method is likely to be infeasible since it is very costly to put the new device in the middle of system operation.

Meanwhile, the latter includes control of the installed power electronics converters, supply side management (SSM), and demand side

management (DSM). SSM includes adjusting output power from microgrid components other than the load. These approaches do not need additional new major devices. Several papers related to this category have been published. In [16], an effective interphase load transfer (ILT) methods are proposed to overcome the voltage unbalance. However, only voltage unbalance is discussed, while other PQ indices are not considered. In [17], three PQ indices are incorporated into the scheduling algorithm. The remedy on the limit violation is based on DSM but applied as iterative methods whose effectiveness is greatly influenced by the multiplier obtained from trial-and-error process. Besides, each PQ index is scanned and treated separately. This may make the PQ handling cumbersome when simultaneous violations on multiple PQ indices limits take place. DSM-based approaches are also used to study the scheduling of a microgrid [18,19]. However, PQ problems are not taken into account. In [20], PQ constraints are incorporated into the optimization. However, the objective function used is the network power loss. It is not indicated whether the proposed algorithm can be adopted for other objective functions or not, considering the most common objective function in the scheduling is the total cost. Moreover, the remedy on PQ indices only depends on the SSM which may not be sufficient in case of intentional islanding. This is also the case in [21], where the optimization is restricted only to minimize voltage total harmonics distortion THD_V at a certain bus. Meanwhile, Ref. [22] only considers THD in the optimization. DSM through load shifting is studied in [23], but only THD is observed. In [24], a day-ahead microgrid scheduling considering several security constraints is proposed. However, the security constraints only include basic quantities such as voltage, current, and power. THD and voltage unbalance are not considered in this study. An attempt to establish a unified PQ index combining different PQ indices is presented in [25], but it has not been tested in any scheduling algorithm.

Control algorithms to handle PQ problems in the microgrid have also been reported in a number of papers. However, the matter of operational cost is not discussed in many studies. In addition, control algorithms mainly deal with supply side in the microgrid. Therefore, DSM is not discussed. In [26], PQ disturbance mitigation is directed towards regulating the negative-sequence voltage in load buses by adjusting negative-sequence voltage at each distributed generation (DG) side. In [27], SSM is carried out through the optimization of BESS and electric vehicle (EV) charging power by using Volt-VAR optimization. It only considers voltage magnitude as the only studied PQ index. SSM is also observed in [28] through power electronics control optimized by gradient descent algorithm. In [29], a central controller optimized by particle swarm optimization (PSO) is proposed, but it only considers THD. Other control scenarios are proposed in [30,31]. However, they also consider THD only. In [32,33], frequency is also considered along with voltage magnitude. However, THD and voltage unbalance are not discussed. Unbalance is addressed in [34], but not THD. Table 1 summarizes and compares the previous works on the operation of microgrid which considers PQ disturbances.

1.3. Research gap & contributions

Based on the comparison presented in Table 1, there is still a need for a DSM-enabled operation scheme of a grid-connected microgrid considering PQ disturbance. DSM is necessary, in addition to BESS and DG power management, to anticipate the intentional islanding operation. This is because during the islanding, the microgrid may lose a significant power imported from the main grid (utility).

This study is aimed at conducting optimal scheduling of power generation in a non-ideal grid-connected microgrid. The original microgrid used in this study is designated to be unbalanced. This is aggravated by the integration of harmonic-producing components at both supply and demand sides. Our main focus, however, is on the harmonics coming from the demand side, which is triggered by various non-linear loads. This addition creates PQ issues in the microgrid, which accordingly adds more constraints to the optimization process. To evaluate these PQ issues, we use three PQ indices, namely (i) voltage magnitude, (ii) voltage THD, and (iii) voltage unbalance factor (VUF). These indices are observed at all load buses in the microgrid under study. In addition to on-grid operation, this study also accommodates the intentional islanding operation within the scheduling framework.

The objectives of this study include the following.

1. To minimize the overall operation cost of the microgrid for 24-hour time horizon through a day-ahead scheduling scheme
2. To avoid PQ indices from violating their limit values within the scheduling framework

The contributions proposed in this study are stated as follows.

1. An iterative optimal harmonic power flow (OHPF) scheme that combines the optimization and harmonic power flow (HPF) processes is constructed. The calculation of important quantities, such as voltage and power loss, takes into account the harmonics components which ensures the accuracy of the obtained results. The existing research works with a similar scheme [17,35] do not either involve HPF or consider harmonics at all stage of calculations even though HPF is used. The iterative process ensures the accurate calculation of the network losses.
2. Within the proposed OHPF, a day-ahead microgrid scheduling incorporating DSM actions based on a flexible combination of load shedding and ILT to avoid the violations on PQ indices limits is presented. These DSM actions are included in the optimization as a set of load constraints.

The remainder of this paper is organized as follows. In Section 2, we discuss in detail the methodology used in this study, which includes the proposed framework and the software implementation. Section 3 contains the description of the test system used in this study. Section 4 explains the case studies. Section 5 presents the results and discussion, while Section 6 gives concluding remarks.

2. Methodology

The heart of this study is OHPF which combines the optimization and HPF algorithms. The optimization, implemented as mixed integer linear programming (MILP) problem, is aimed at minimizing the total operational cost of the microgrid and HPF is to calculate PQ indices and check if they are within the permissible limits. The proposed OHPF framework is illustrated by the flowchart shown in Fig. 1. The description of the optimization and HPF constituting the proposed OHPF framework is presented below.

2.1. The optimization formulation

The development of OHPF framework starts with the optimization, which schedules both active and reactive powers in the microgrid. When several DG technologies and other additional components are integrated into the microgrid, the goal of the optimization is to minimize the total operational cost. Meanwhile, the constraints related to PQ indices are to be incorporated in the form of the penalty function. In this study, the objective function consists of two components, including the total cost function and the penalty function. That is

$$\min J = F + \text{Penalty} \tag{1}$$

where F is the total cost function, which is expressed as follows,

$$F = \underbrace{\sum_t \sum_i C_i^{\text{st}} v_i(t)}_{\substack{\text{startup cost of}\\ \text{dispatchable units}}} + \underbrace{\sum_t \sum_i C_i^{\text{op}} p_i(t) u_i(t)}_{\substack{\text{operational cost of}\\ \text{dispatchable units}}} + \underbrace{\sum_t p_{\text{grid}}^{\text{in}}(t) C_{\text{grid}}^{\text{in}}(t)}_{\substack{\text{cost of importing}\\ \text{energy from grid}}} -$$
$$\underbrace{\sum_t p_{\text{grid}}^{\text{out}}(t) C_{\text{grid}}^{\text{out}}(t)}_{\substack{\text{revenue from exporting}\\ \text{energy to grid}}} + \underbrace{\sum_t \sum_l \left(P_l(t) - p_l(t)\right) C_l^{LS}}_{\text{cost of load shedding}} - \underbrace{C_{\text{B}}^{\text{res}} soe_{\text{B}}(T)}_{\substack{\text{revenue from soe of}\\ \text{BESS in final hour}}} +$$

Table 1
Comparison of reviewed papers on optimization and/or control of microgrid considering PQ.

Ref.	Power Flow	PQ Index[a]			PQ Handling Technique	Harmonics in Losses	Mode of Operation[b]		Time Series
		Volt.	THD	VU			On-grid	Stand-alone	
[8]	×	✓	✓	×	Optimized passive filters	n/a	✓	×	✓
[9]	✓	✓	✓	✓	Optimized passive filters	✓	✓	×	×
[10]	✓	✓	×	×	Optimized D-STATCOM	×	✓	×	✓
[11]	×	✓	✓	×	Virtual admittance and impedance	×	✓	×	✓
[12]	✓	✓	✓	×	Optimized virtual impedances of the DGs	×	✓	×	✓
[13]	×	✓	✓	×	D-STATCOM with optimally-tuned PID controller	×	×	✓	✓
[14]	×	✓	✓	×	Cost-function-based control optimized by MPC	×	×	✓	✓
[15]	×	✓	✓	×	Optimization of hybrid control scheme-based active filter	n/a	✓	×	✓
[16]	✓	×	×	✓	Iterative DSM through ILT	n/a	✓	×	✓
[17]	✓	✓	✓	✓	Iterative DSM through load shedding & ILT	×	✓	×	✓
[20]	✓	✓	✓	✓	BESS power optimization via PSO	✓	✓	×	✓
[21]	✓	✓	✓	×	Optimized active filter	n/a	✓	×	×
[22]	✓	✓	✓	×	DSM through load shedding	n/a	✓	×	✓
[23]	×	×	✓	×	DSM through load shifting	×	×	✓	✓
[24]	✓	✓	×	×	BESS and DGs power optimization	×	✓	×	✓
[26]	×	✓	×	×	Voltage regulation through adjustment of negative-sequence voltage at DG side	×	✓	×	✓
[27]	✓	✓	×	×	BESS & EV charging power optimization via hierarchical Volt-VAR optimization	×	✓	×	✓
[28]	×	✓	✓	✓	PQ controller with plug-and-play structure optimized by gradient descent algorithm	×	×	✓	✓
[29]	×	×	✓	×	Harmonics minimization through DG voltage adjustment	×	×	✓	✓
[30]	×	✓	✓	×	Harmonic compensation & power control via current-based control algorithm	×	✓	×	✓
[31]	×	✓	✓	×	Adaptive filtering with momentum based least mean square control	×	✓	×	✓
[32]	✓	✓	×	×	BESS power adjustment via DEO-ANN controller	×	✓	×	✓
[34]	✓	✓	×	✓	DG power control via three-layer hierarchical control	×	✓	×	✓
This study	✓	✓	✓	✓	DSM through flexible combination of load shedding & ILT	✓	✓	×	✓

Note: VU = voltage unbalance, n/a = not available

[a] Current and TDD are deemed analogous to voltage and THD

[b] Intentional islanding can also be made possible within on-grid (grid-connected) mode.

$$\underbrace{\sum_t C_{\mathrm{B}}^{\mathrm{deg}}\left(p_{\mathrm{B}}^{\mathrm{ch}}(t)+p_{\mathrm{B}}^{\mathrm{dch}}(t)\right)}_{\text{BESS degradation cost}}+\underbrace{\sum_t\sum_k C_{\mathrm{EV}}^{\mathrm{deg}}\left(p_{\mathrm{EV},k}^{\mathrm{ch}}(t)+p_{\mathrm{EV},k}^{\mathrm{dch}}(t)\right)}_{\text{EV battery degradation cost}}+\underbrace{\sum_t C_{\mathrm{grid}}^{Q}\left(q_{\mathrm{grid}}^{\mathrm{in}}(t)+q_{\mathrm{grid}}^{\mathrm{out}}(t)\right)}_{\text{penalty for reactive power exchange with grid}}$$
$$+\underbrace{\sum_t C_{\mu}^{Q}\left(\sum_i\left(q_i^{\mathrm{gen}}(t)+q_i^{\mathrm{abs}}(t)\right)+q_{\mathrm{B}}^{\mathrm{gen}}(t)+q_{\mathrm{B}}^{\mathrm{abs}}(t)+q_{\mathrm{WT}}^{\mathrm{gen}}(t)+q_{\mathrm{WT}}^{\mathrm{abs}}(t)+q_{\mathrm{PV}}^{\mathrm{gen}}(t)+q_{\mathrm{PV}}^{\mathrm{abs}}(t)\right)}_{\text{penalty for reactive power exchange among microgrid components}} \quad (2)$$

The last two terms in the cost function represent cost components aimed at minimizing reactive power flow within the microgrid and between the microgrid and main grid. This minimization is to avoid excessive power losses in the distribution cables [17]. Meanwhile, the penalty function is given below.

$$\text{Penalty}=\underbrace{\lambda_V\left[\sum_t\sum_l\sum_f\left(\max\left\{0,\left(V_{l,f}(t)-V^{\max}\right)\right\}\right)^2+\left(\max\left\{0,\left(V^{\min}-V_{l,f}(t)\right)\right\}\right)^2\right]}_{\text{penalty function for voltage magnitude}}+$$
$$\underbrace{\lambda_{\mathrm{THD}}\sum_t\sum_l\sum_f\left(\max\left\{0,\left(\mathrm{THD}_{l,f}(t)-\mathrm{THD}^{\max}\right)\right\}\right)^2}_{\text{penalty function for voltage THD}}+$$
$$\underbrace{\lambda_{\mathrm{VUF}}\sum_t\sum_l\left(\max\left\{0,\left(\mathrm{VUF}_l(t)-\mathrm{VUF}^{\max}\right)\right\}\right)^2}_{\text{penalty function for voltage VUF}} \quad (3)$$

A value of 10^{-6} is assigned to λ_V, λ_{THD}, and λ_{VUF}.

The penalty function method converts the constrained optimization problem into an unconstrained one. It will not in any case improve power quality indices (voltage magnitudes, THD_V, and VUF). It will constrain them in a predefined range. Using (3), each unsatisfied constraint influences the solution (i.e., the set of design variables) by assessing a penalty equal to the square of the violation. These influences are summed and multiplied by λ_V, λ_{THD}, and λ_{VUF}, the penalty

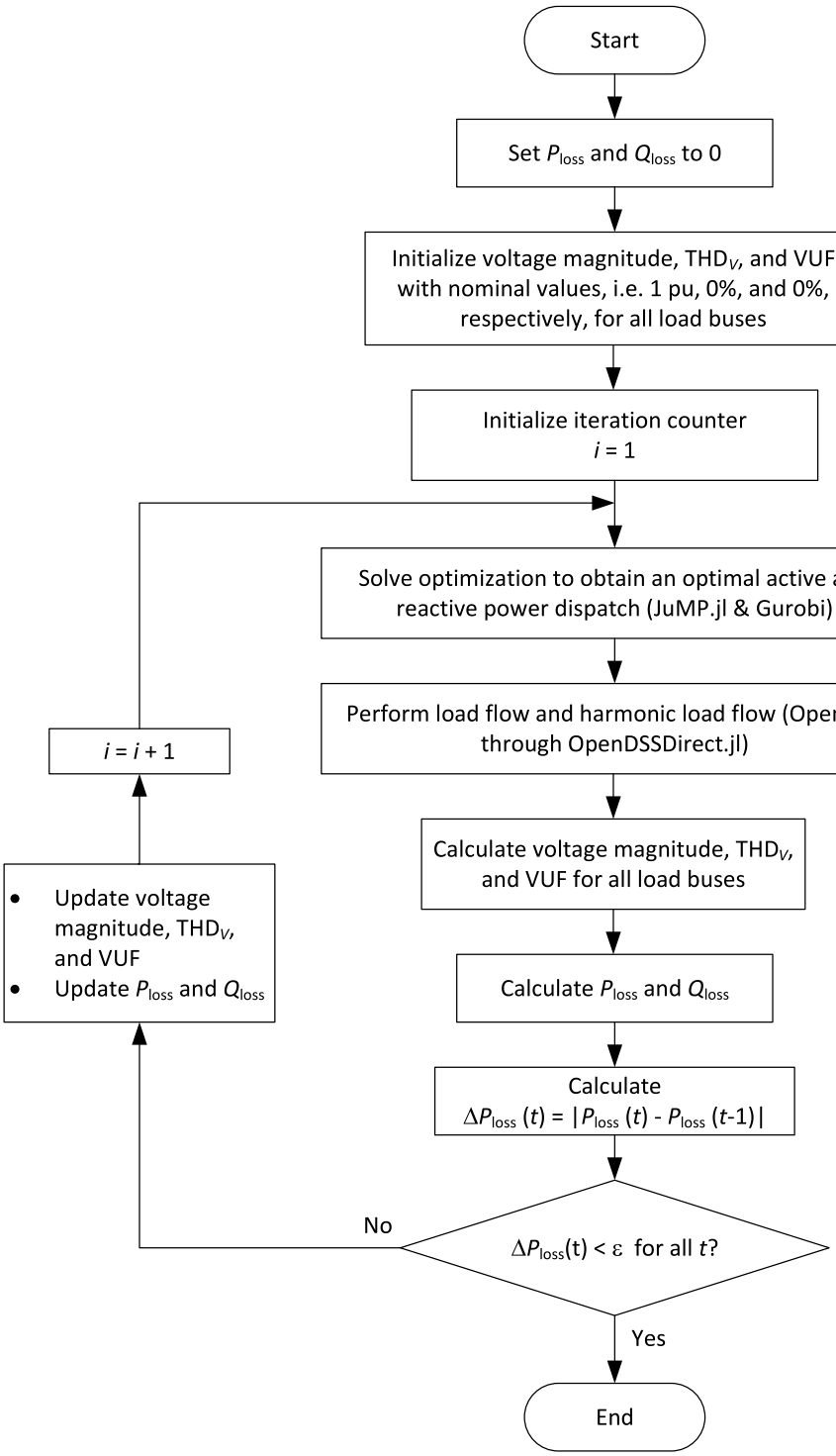

Fig. 1. Flowchart of the proposed OHPF.

coefficients which are positive constants that control how strongly the constraints will be enforced. From (3) it can be seen that this influence is counterbalanced by F. In general, if the values of λ_V, λ_{THD}, and λ_{VUF} are made properly large, the penalty term will exact such a heavy cost for any constraint violation that the minimization of the augmented objective function J will yield a feasible solution. However, one may think that all we need to do is to set λ_V, λ_{THD}, and λ_{VUF} to a very large value and then optimize the resulting augmented objective function J to obtain the optimal solution. Unfortunately, this is not true. A systematic way to determine the values of the penalty coefficients is to start with a relatively small value of λ_V, λ_{THD}, and λ_{VUF} and then subsequently, solve a sequence of unconstrained problems with monotonically increasing values of these parameters chosen so that the solution to each new problem is "close" to the previous one and continue this process until we obtain a sufficiently accurate minimum. A relatively small value of the penalty coefficients can be accepted provided the obtained solutions are good enough.

The values of $V_{l,f}$, $THD_{l,f}$, and VUF_l in (3) are unknown before the optimization process at the first iteration; therefore, they are initiated with the nominal values of 1 pu, 0%, and 0%, respectively. These values are then updated by HPF in OpenDSS [36], as shown in Fig. 1.

One may use a different objective function for the framework presented in Fig. 1. We use the total operational cost since this is the most common quantity in the microgrid optimization [37]. The network power loss may also be opted as the objective function [20]. However, since the ultimate goal is also to minimize the cost, choosing the operational cost is more direct and effective to attain such a goal.

The minimization of the objective function in (1) is subject to the following constraints.

1. Power balance constraints:

$$\sum_i p_i(t) + P_{\mathrm{WT}}(t) + P_{\mathrm{PV}}(t) + p_{\mathrm{B}}^{\mathrm{dch}}(t) + \sum_k p_{\mathrm{EV},k}^{\mathrm{dch}}(t) + p_{\mathrm{grid}}^{\mathrm{in}}(t) = \sum_l p_l(t) + p_{\mathrm{B}}^{\mathrm{ch}}(t) + \sum_k p_{\mathrm{EV},k}^{\mathrm{ch}}(t) + p_{\mathrm{grid}}^{\mathrm{out}}(t) + p^{\mathrm{loss}}(t) \quad \forall t \tag{4}$$

$$\sum_i q_i^{\mathrm{gen}}(t) + q_{\mathrm{B}}^{\mathrm{gen}}(t) + q_{\mathrm{WT}}^{\mathrm{gen}}(t) + q_{\mathrm{PV}}^{\mathrm{gen}}(t) + q_{\mathrm{grid}}^{\mathrm{in}}(t) = \sum_i q_i^{\mathrm{abs}}(t) + \sum_l q_l(t) + q_{\mathrm{B}}^{\mathrm{abs}}(t) + q_{\mathrm{WT}}^{\mathrm{abs}}(t) + q_{\mathrm{PV}}^{\mathrm{abs}}(t) + q_{\mathrm{grid}}^{\mathrm{out}}(t) + q^{\mathrm{loss}}(t) \quad \forall t \tag{5}$$

2. Load and DSM constraints:

$$P_{l,f}^{\min}(t) \le p_{l,f}(t) \le P_{l,f}^{\max}(t) \quad \forall l, \forall t \tag{6}$$

$$q_{l,f}(t) = \frac{\sqrt{1 - PF_{l,f}^2}}{PF_{l,f}} p_{l,f}(t) \quad \forall l, \forall t \tag{7}$$

$$p_l(t) = \sum_f p_{l,f}(t) \quad \forall l, \forall t \tag{8}$$

In this study, we propose two DSM schemes based on the idea of enabling a flexible combination of load shedding and ILT. The latter is to achieve a good load distribution among the three phases. These schemes, tagged as DSM Scheme 1 and DSM Scheme 2, are formulated by adjusting the values of $P_{l,f}^{\min}$ and $P_{l,f}^{\max}$ for the constraint in (6). The value of $P_{l,f}^{\min}$ for both schemes are as follows.

$$P_{l,f}^{\min(1)}(t) = \begin{cases} P_{l,f}(t) & \text{for } P_{l,f}(t) < (1/3)P_l(t) \quad \forall l, \forall f, \forall t \\ (1/3)P_l(t) & \text{otherwise} \quad \forall l, \forall f, \forall t \end{cases} \tag{9a}$$

$$P_{l,f}^{\min(2)}(t) = \begin{cases} 0 & \text{for } P_{l,f}(t) < (1/3)P_l(t) \quad \forall l, \forall f, \forall t \\ (1/3)P_l(t) & \text{otherwise} \quad \forall l, \forall f, \forall t \end{cases} \tag{9b}$$

Note that, DSM Scheme 1 gives a tighter lower bound through the constraint in (9a) than that of DSM Scheme 2 in the constraint in (9b). Consequently, DSM Scheme 2 may result in higher cost of load shedding but a possible better performance in mitigating PQ disturbances. Meanwhile, the value of $P_{l,f}^{\max}$ is given below.

$$P_{l,f}^{\max}(t) = \begin{cases} P_{l,f}(t) & \text{for } P_{l,f}(t) > (1/3)P_l(t) \quad \forall l, \forall f, \forall t \\ (1/3)P_l(t) & \text{otherwise} \quad \forall l, \forall f, \forall t \end{cases} \tag{10}$$

The constraint in (10) is applicable to both DSM schemes. They are only distinguished by the lower bound of the load demand in the constraint in (9). The aim of the constraints in (9)–(10) is to enforce the load distribution among the three phases as equal as possible. Meanwhile, the flexibility in carrying out load shedding is accommodated by the following constraint expression.

$$\sum_f p_{l,f}(t) \le P_l(t) \quad \forall l, \forall t \tag{11}$$

3. Dispatchable (diesel) unit constraints:

$$u_i(t)P_i^{\min} \le p_i(t) \le u_i(t)P_i^{\max} \quad \forall i, \forall t \tag{12}$$

$$0 \le q_i^{\mathrm{gen}}(t), q_i^{\mathrm{abs}}(t) \le (1 - s(t))Q_i^{\max} \quad \forall i, \forall t \tag{13}$$

$$v_i(t) - w_i(t) = u_i(t) - u_i(t-1) \quad \forall i, \forall t \tag{14}$$

$$v_i(t) + w_i(t) \le 1 \quad \forall i, \forall t \tag{15}$$

$$s(t) \le \frac{1}{3}(u_i(t-1) + u_i(t) + u_i(t+1)) \quad \forall i, \forall t \tag{16}$$

All dispatchable units are assumed to be off before the scheduling period, i.e., $u_i(0) = 0$. Also, the constraint in (16) is intended to utilize the dispatchable unit for smooth transition between grid-connected and stand alone modes [38].

4. WT and PV contraints:

$$0 \le q_{\mathrm{WT}}^{\mathrm{gen}}(t), q_{\mathrm{WT}}^{\mathrm{abs}}(t) \le Q_{\mathrm{WT}}^{\max} \quad \forall t \tag{17}$$

$$0 \le q_{\mathrm{PV}}^{\mathrm{gen}}(t), q_{\mathrm{PV}}^{\mathrm{abs}}(t) \le Q_{\mathrm{PV}}^{\max} \quad \forall t \tag{18}$$

5. BESS constraints:

$$0 \le p_{\mathrm{B}}^{\mathrm{ch}}(t) \le u_{\mathrm{B}}^{\mathrm{ch}}(t)P_{\mathrm{B}}^{\max} \quad \forall t \tag{19}$$

$$0 \le p_{\mathrm{B}}^{\mathrm{dch}}(t) \le u_{\mathrm{B}}^{\mathrm{dch}}(t)P_{\mathrm{B}}^{\max} \quad \forall t \tag{20}$$

$$soe_{\mathrm{B}}(t) = SOE_{\mathrm{B}}^{\mathrm{init}} + \eta_{\mathrm{B}}p_{\mathrm{B}}^{\mathrm{ch}}(t) - \frac{p_{\mathrm{B}}^{\mathrm{dch}}(t)}{\eta_{\mathrm{B}}} \quad \forall t = 1 \tag{21}$$

$$soe_{\mathrm{B}}(t) = soe_{\mathrm{B}}(t-1) + \eta_{\mathrm{B}}p_{\mathrm{B}}^{\mathrm{ch}}(t) - \frac{p_{\mathrm{B}}^{\mathrm{dch}}(t)}{\eta_{\mathrm{B}}} \quad \forall t \in [2, T] \tag{22}$$

$$SOE_{\mathrm{B}}^{\min} \le soe_{\mathrm{B}}(t) \le SOE_{\mathrm{B}}^{\max} \quad \forall t \tag{23}$$

$$soe_{\mathrm{B}}(T) \ge SOE_{\mathrm{B}}^{\mathrm{init}} \tag{24}$$

$$0 \le q_{\mathrm{B}}^{\mathrm{gen}}(t), q_{\mathrm{B}}^{\mathrm{abs}}(t) \le \frac{\sqrt{1 - PF_{\mathrm{B}}^2}}{PF_{\mathrm{B}}} P_{\mathrm{B}}^{\max} \quad \forall t \tag{25}$$

$$u_{\mathrm{B}}^{\mathrm{ch}}(t) + u_{\mathrm{B}}^{\mathrm{dch}}(t) \le 1 \quad \forall t \tag{26}$$

6. EV constraints:

$$0 \le p_{\mathrm{EV},k}^{\mathrm{ch}}(t) \le u_{\mathrm{EV},k}^{\mathrm{ch}}(t)P_{\mathrm{EV}}^{\max} \quad \forall k, \forall t \in \left[T_{\mathrm{EV}}^{\mathrm{arr}}, T_{\mathrm{EV}}^{\mathrm{dep}}\right] \tag{27}$$

$$0 \le p_{\mathrm{EV},k}^{\mathrm{dch}}(t) \le u_{\mathrm{EV},k}^{\mathrm{dch}}(t)P_{\mathrm{EV}}^{\max} \quad \forall k, \forall t \in \left[T_{\mathrm{EV}}^{\mathrm{arr}}, T_{\mathrm{EV}}^{\mathrm{dep}}\right] \tag{28}$$

$$soe_{\mathrm{EV},k}(t) = SOE_{\mathrm{EV},k}^{\mathrm{init}} + \eta_{\mathrm{EV}}p_{\mathrm{EV},k}^{\mathrm{ch}}(t) - \frac{p_{\mathrm{EV},k}^{\mathrm{dch}}(t)}{\eta_{\mathrm{EV}}} \quad \forall k, \forall t = T_{\mathrm{EV}}^{\mathrm{arr}} \tag{29}$$

$$soe_{\mathrm{EV},k}(t) = soe_{\mathrm{EV},k}(t-1) + \eta_{\mathrm{EV}}p_{\mathrm{EV},k}^{\mathrm{ch}}(t) - \frac{p_{\mathrm{EV},k}^{\mathrm{dch}}(t)}{\eta_{\mathrm{EV}}} \quad \forall k, \forall t \in \left(T_{\mathrm{EV}}^{\mathrm{arr}}, T_{\mathrm{EV}}^{\mathrm{dep}}\right] \tag{30}$$

$$SOE_{\mathrm{EV}}^{\min} \le soe_{\mathrm{EV},k}(t) \le SOE_{\mathrm{EV}}^{\max} \quad \forall k, \forall t \in \left[T_{\mathrm{EV}}^{\mathrm{arr}}, T_{\mathrm{EV}}^{\mathrm{dep}}\right] \tag{31}$$

$$soe_{\mathrm{EV},k}(t) \ge SOE_{\mathrm{EV},k}^{\mathrm{init}} \quad \forall k, \forall t = T_{\mathrm{EV},k}^{\mathrm{dep}} \tag{32}$$

$$u_{\mathrm{EV},k}^{\mathrm{ch}}(t) + u_{\mathrm{EV},k}^{\mathrm{dch}}(t) \le 1 \quad \forall k, \forall t \in \left[T_{\mathrm{EV}}^{\mathrm{arr}}, T_{\mathrm{EV}}^{\mathrm{dep}}\right] \tag{33}$$

7. Grid interaction constraints:

$$p_{\mathrm{grid}}^{\mathrm{in}}(t), p_{\mathrm{grid}}^{\mathrm{out}}(t) \le (1 - s(t))P_{\mathrm{grid}}^{\max} \quad \forall t \tag{34}$$

$$q_{\mathrm{grid}}^{\mathrm{in}}(t), q_{\mathrm{grid}}^{\mathrm{out}}(t) \le (1 - s(t))Q_{\mathrm{grid}}^{\max} \quad \forall t \tag{35}$$

It is noted from Fig. 1 that while the calculation of the network losses is an iterative process, the DSM itself is basically not an iteration. It just follows the iterative process required by the losses calculation.

2.2. Harmonic power flow framework

HPF is used to anticipate the presence of non-linear loads in the microgrid system. The main PQ problem caused by non-linear loads is the harmonic which distorts the pure sine waves. The harmonics also influence the voltage magnitude and power loss. HPF calculates and quantifies this issue by modeling non-linear loads with current harmonic sources for certain spectra.

The optimization cannot directly solve for the network power losses. Thus, the power losses are initially set to zero. The values of the scheduled power produced by the optimization are then fed to HPF algorithm to be used for calculation of quantities such as voltages at all load buses, power at all components, and power losses at all harmonic frequency spectra. At this stage, there will be mismatches between the initial guess of power losses and the losses calculated by HPF. The power losses calculated by HPF are then sent back to the optimization algorithm for re-scheduling. This iteration stops when the mismatches between losses calculated by HPF at a certain iteration and those at the preceding iteration at all hours are less than a certain error ϵ. In this study, we use a stopping error ϵ of 1 kW.

There are three PQ indices observed in this study. The first index is the voltage magnitude at load buses. Under the presence of harmonics, the voltage calculation should consider the components at frequencies other than the fundamental. It is expressed as follows.

$$V = \sqrt{\sum_{n=1}^{h} V_n^2} \tag{36}$$

where h is the highest harmonic order considered in the study. In terms of voltage magnitude, the system is considered healthy if voltage magnitudes at all load buses are within standard limits, i.e., between 0.95 pu and 1.05 pu.

The second index is the voltage THD, which is calculated as follows.

$$\mathrm{THD}_V = \frac{\sqrt{\sum_{n=2}^{h} V_n^2}}{V_1} \times 100 \tag{37}$$

A multiplier of 100 is added to express THD_V as a percentage. We use a limit of 5% for THD_V assessment in each load bus. Thus, THD_V higher than 5% is considered above the limit and should be remedied.

The last observed index is the voltage unbalance, which is expressed in terms of voltage unbalance factor (VUF) and is calculated by using IEEE true definition formula [20] as follows.

$$\mathrm{VUF} = \frac{V^-}{V^+} \times 100 \tag{38}$$

where V^- is the negative sequence component of the voltage measured at a certain bus and V^+ is its positive sequence component. VUF is only calculated at fundamental frequency [20]. As per IEEE criterion [39], VUF should not exceed 2%. Severe VUF limit violation may require ILT to achieve a better load demand distribution [16].

These PQ indices are independent, which means that the violation on one index does not necessarily bring impact on the other indices. Based on this fact, many existing research in PQ handle the violations on PQ indices separately. In this paper, we propose an integrated handling of PQ indices limits violations under OHPF scheme that we have described. As three PQ indices are considered in this study, there are eight possible events that can be experienced by the system as shown in Table 2. Based on this list, Event 7 is the most severe condition on the system since all PQ indices experience limit violation. On the other hand, Event 0 represents a healthy system where there is no PQ limits violation. Thus, we can simply relegate it from PQ restorative actions.

Instead of handling each PQ index separately, in this study we propose a DSM-based approach integrated to the OHPF through a set of optimization constraints. In this scheme, the microgrid operator and consumers agree on specific contracts and tariffs with the possibility of controlling consumers' consumption. This flexible load shaping (through load shedding action if necessary) is compensated by applying a load shedding cost. This cost is to be paid by the microgrid operator to the consumers whenever there is a reduction on the power supply from the demand forecast. It has been integrated into the overall cost formulation in (1).

Table 2
Possible events caused by different combinations of the limit violations on PQ indices.

Event	Violation on V	Violation on THD_V	Violation on VUF
0	×	×	×
1	×	×	✓
2	×	✓	×
3	✓	×	×
4	×	✓	✓
5	✓	✓	×
6	✓	×	✓
7	✓	✓	✓

2.3. Software implementation

The framework shown in Fig. 1 is implemented in Julia programming language by using JuMP.jl [40] and is solved by Gurobi [41] through Gurobi.jl interface. Meanwhile, HPF is implemented in and solved by OpenDSS, which is invoked by OpenDSSDirect.jl. OpenDSSDirect.jl is a Julia package that implements a direct library interface to OpenDSS. It can be faster to drive OpenDSS from this interface than from the traditional COM interface. The calculation of PQ indices in (36)–(38) is also carried out in Julia utilizing the values of all harmonic spectra obtained from OpenDSS.

3. Test system

Throughout this study, we utilize the modified IEEE 37-bus test feeder [42]. The system is modified by incorporating several distributed generators (DGs) and BESS. In addition, the system is made ready for electric vehicle (EV) charging station integration. Thus, the modified system is subject to charging–discharging cycles during its scheduling period. The single line diagram of the modified system is shown in Fig. 2. In the modified system, two identical diesel engine (DE) units are connected to bus 701, wind turbine (WT) units are connected to bus 722, solar photovoltaic (PV) units are connected to bus 730, BESS is connected to bus 720, and EV charging station is connected to bus 737. The data of these additional components and the grid electricity price (buying and selling) are taken from [17]. However, the size of DE and power forecast of WT and PV have been doubled to adjust for the demand level. Fig. 3 shows the load shape and the forecast output power of renewable/non-dispatchable DGs used by the system.

These additional components (except DE) are inverter-based, thus harmonic injection is the direct consequence of their integration. We model the harmonics injection of these components by specifying their odd harmonic current. Table 3 shows the spectra of harmonic current injection of WT and PV, while Table 4 is for those of EV and BESS.

The loading of the system is unbalanced, which is suitable for PQ-related studies. To accommodate a time-series study, we modify the loading level at all load buses according to the load shape shown in the upper part of Fig. 3. In this case, the original load of the system is deemed as the peak load. This load shape is based on the normalized value of real-time demand at 15 November 2022, taken from [45]. Furthermore, for the sake of simplification, all spot loads are modeled as constant PQ loads.

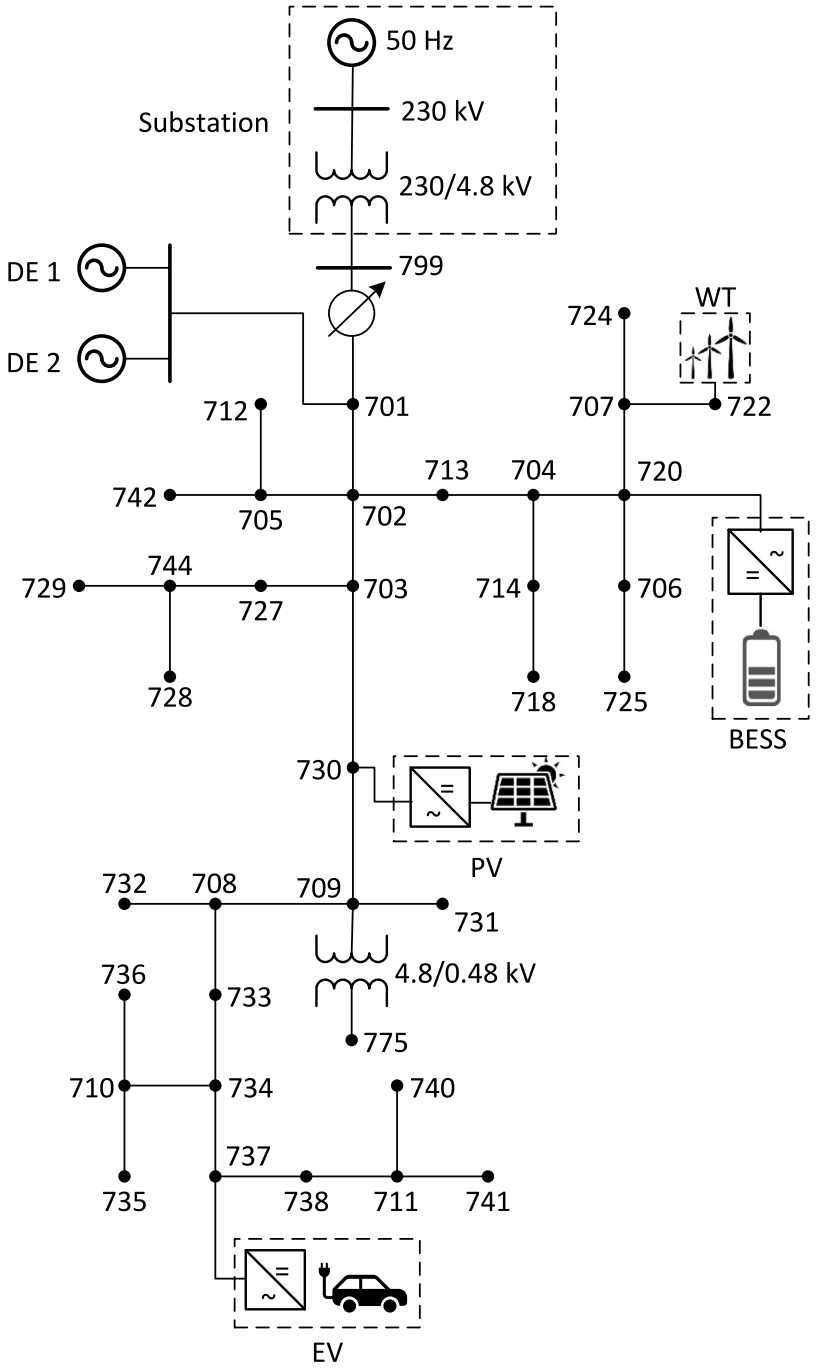

Fig. 2. IEEE 37-bus feeder with DGs, BESS, and EV charging station.

Table 3
Harmonic current injection of WT and PV [9].

Harmonic Order	Magnitude (%)	Phase (^{0})
1	100	−2.34
3	20	−15.29
5	15	−20.74
7	10	−30.85
9	8	140.36
11	5	65.54
13	3	42.62
15	2	153.28

Table 4
Harmonic current injection of BESS and EV [43,44].

Harmonic Order	Magnitude (%)	Phase (^{0})
1	100	−26
3	31	−52
5	25	−94
7	17	−67
9	14	−66
11	9	−67
13	5	−46
15	3	−56

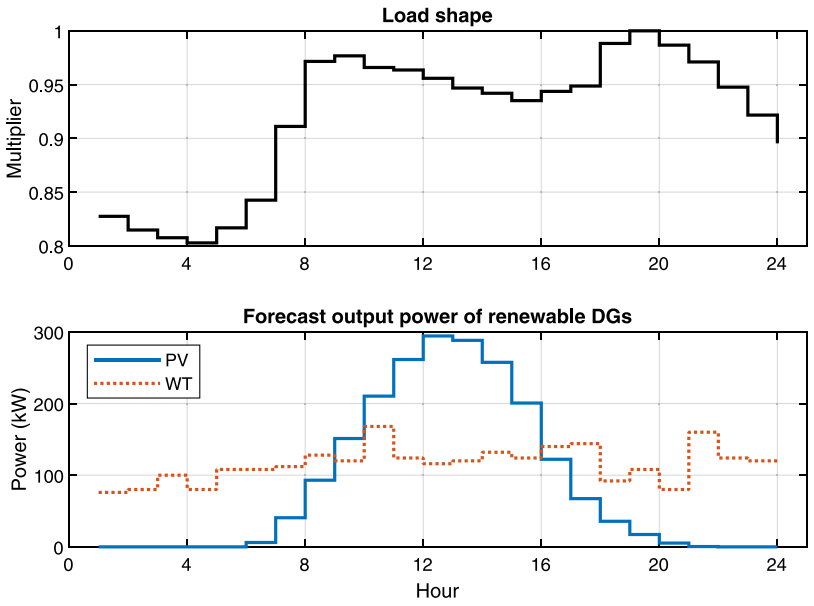

Fig. 3. Load shape and renewable DGs forecast output power for the utilized IEEE 37-bus system.

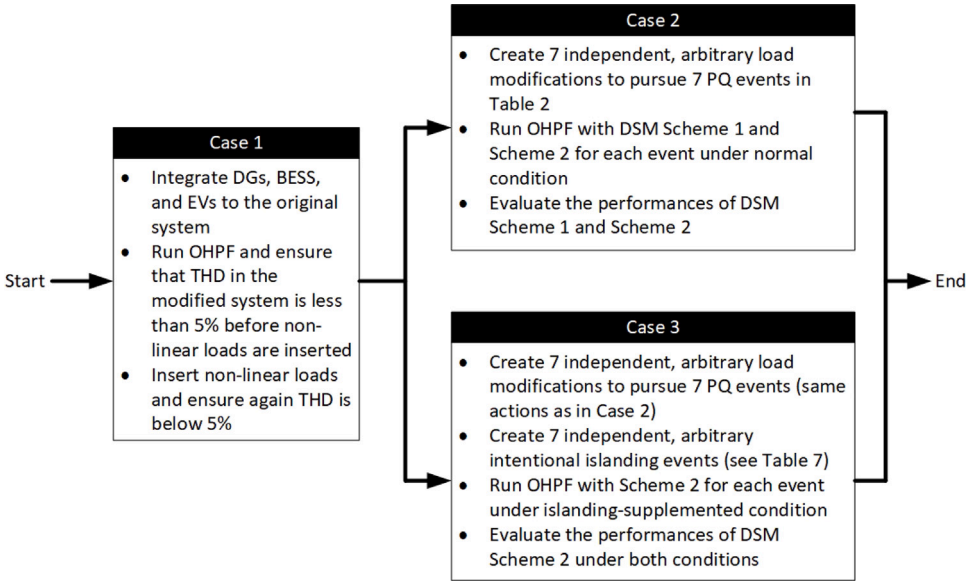

Fig. 4. Block diagram of the cases.

4. Case studies

The study is divided into three cases, namely Case 1, Case 2, and Case 3, representing three different purposes. All cases are time-series with 24-hour time horizon, therefore load shape in Fig. 3 is applied in all cases. The relationship among these three cases are depicted by the block diagram in Fig. 4.

The description for each case is given as follows.

4.1. Case 1

Case 1 is intended for achieving the disturbance-free integration of DGs, BESS, and EV into the microgrid. It is also to include the composite load. The resulting microgrid configuration will be the basis for Case 2. It is carried out in three sub-cases tagged as Case 1a, Case 1b, and Case 1c. Case 1b is the continuation of Case 1a and Case 1c is the continuation of Case 1b. In other words, the microgrid configuration in Case 1c accumulates those in Case 1a and Case 1b. Their descriptions are presented in Fig. 5. It is to be noted that there is no load fluctuation in Case 1, which means that the total load demand pattern used is the one shown in Fig. 3. The modification of load composition in Case 1c does not change the total load demand.

In Case 1a, the integration of DGs, BESS, and EV obviously create harmonics in the microgrid and THD limit is likely to be violated. Case 1b is intended to suppress these harmonics. In Case 1b, we adopt the method described in [46] to determine the size of single-tuned filter (STF) for the system. STF is used to reduce THD_V since it is the most economical technique. DSM is not carried out at this point since the harmonics only come from the supply side.

Meanwhile, the designated buses for the placement of composite loads in Case 1c include bus 712, bus 718, bus 728, bus 736, and bus 741. The load compositions for these buses are given in Table 5. The

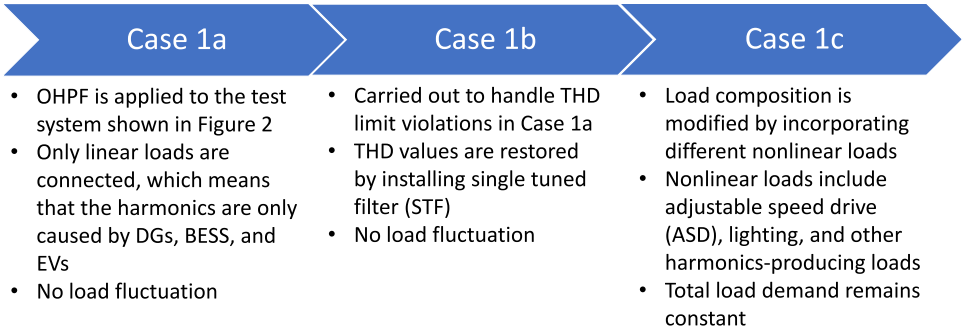

Fig. 5. Description of Case 1.

Table 5
Load compositions for buses with composite loads [9].

Bus	Linear (%)	Lighting (%)	ASD (%)	Other (%)
712	10	25	60	5
718	5	15	70	10
728	20	60	10	10
736	10	20	65	5
741	15	50	30	5

Table 6
Harmonic spectra of the harmonic-producing load types used in the study [9].

Harmonic	ASD		Lighting		Other	
Order	Mag (%)	Phase (^{0})	Mag (%)	Phase (^{0})	Mag (%)	Phase (^{0})
1	100	−1.45	100	−107	100	105.5
3	84.6	−8.34	19.2	76	3.6	−44.4
5	68.3	−14.23	10.7	10	3.2	139
7	47.8	−20.13	2.1	37	0	0
9	27.7	−29.02	1.4	31	0	0
11	0.2	−27.91	0.9	36	0	0
13	6.1	158.2	0.6	47	0	0
15	4.2	122.3	0.5	20	0	0
THD_I	122.1846		22.1567		4.8166	

load types that make up the composite loads include the linear load, lighting load, adjustable speed drive (ASD) load, and other harmonic-producing loads (not specified). The assumed cost of load shedding for these four types of load in this study are 0.2 $/kWh, 0.55 $/kWh, 0.85 $/kWh, and 0.55 $/kWh, respectively. The linear load is the original system load, which does not inject harmonic current. The remaining load types are the source of harmonics current, but with different spectra. The harmonic spectra of all harmonic-producing load types are presented in Table 6. ASD is the most-polluting load type since its current THD is the highest.

4.2. Case 2

The microgrid configuration resulting from Case 1 (which is accumulated in Case 1c) is the base for Case 2, as previously indicated. Utilizing the system configuration constructed in Case 1c, we designate here Case 2 for accommodating different load fluctuations. The load fluctuations/variations are intended to pursue the seven events listed in Table 2. The process for making these variations is arbitrary in order to assess the effectiveness of the proposed framework. To match the number of PQ events listed in Table 2, Case 2 is divided into seven sub-cases from Case 2a to Case 2 g. These load variations can be in terms of load demand level, harmonic spectra, or both. The detailed variations for these cases are presented in Fig. 6. It is again asserted that the base for the action described for each sub-case in Fig. 6 is the microgrid configuration in Case 1c, not in preceding sub-case. That is, each sub-case of Case 2 is independent of other sub-cases.

Table 7
The period of the intentional islanding in Case 3.

Sub-Case	Period for intentional islanding
Case 3a	From $t = 3$ to $t = 6$
Case 3b	From $t = 14$ to $t = 17$
Case 3c	From $t = 11$ to $t = 14$
Case 3d	From $t = 17$ to $t = 20$
Case 3e	From $t = 5$ to $t = 9$
Case 3f	From $t = 9$ to $t = 12$
Case 3g	From $t = 15$ to $t = 18$

4.3. Case 3

In Case 2, the decision on whether the power flow between the microgrid and the main grid should take place or not is governed by the decision binary variable s. When $s = 1$, the microgrid is disconnected from the main grid, i.e., the islanding takes place. Otherwise, the microgrid is connected to the main grid and the power flow between them occurs. In other words, this decision is determined by the optimization process during the entire scheduling period.

In the subsequent case, we introduce the intentional islanding for a portion of scheduling period. The load fluctuations are exactly same as those in Case 2 (Fig. 6). The only difference is that in in this case we apply the intentional islanding by forcing the power flow between the microgrid and the main grid to be zero. To make differentiation, this case with the intentional islanding is named as Case 3, which is also constituted by seven sub-cases, but now tagged as Case 3a to Case 3 g. The intentional islanding is temporary and the choice for this islanding period is again arbitrary. They are presented in Table 7.

5. Results and discussion

We present the results based on different cases explained in the preceding section and also in accordance with the PQ events listed in Table 2. The discussions are based on the three PQ indices (voltage magnitude, THD_V, and VUF) resulting from the simulation using the proposed OHPF framework.

5.1. Case 1

Fig. 7 shows the simulation results for Case 1 comprising minimum and maximum voltage magnitudes, maximum voltage THD, and maximum VUF. In Case 1a, out of four quantities under monitoring, limit violation is detected for voltage THD. Its maximum values for 24 h exceed the limit of 5%, which is a quite severe disturbance. Thus, filter addition (Case 1b) should be carried out.

Based on several experiments, it is found that four 200-kVAR STFs tuned at 9th harmonic are sufficient to suppress the harmonics and reduce the voltage THD accordingly. These STFs are installed at bus 722, bus 724, bus 740, and bus 741. The results are shown in Fig. 7, where voltage THD values are now under control without disturbing other PQ indices. Therefore, we move forward with this filter configuration. In

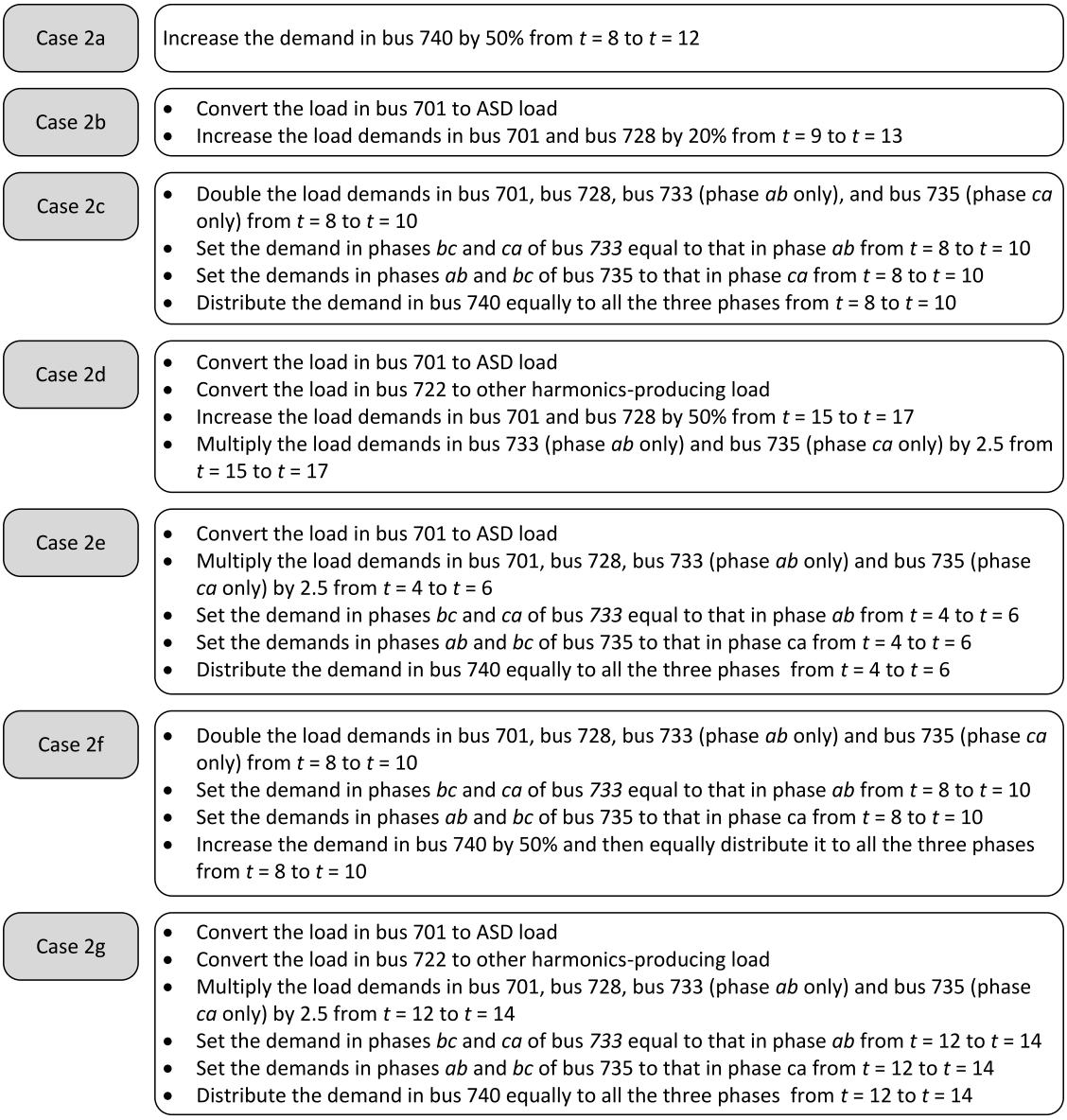

Fig. 6. Actions to pursue Case 2.

other words, it is assumed that these STFs are installed permanently before the scheduling starts.

In Case 1c, with the inclusion of different non-linear loads, we observe the increase of voltage THD values. However, the values are still well below 5%, prompting no further action at this state. This is the base configuration before any load variations are made in Case 2.

5.2. Case 2

As previously indicated, we divide Case 2 into seven different sub-cases, namely Case 2a to Case 2 g, to pursue Event 1 to Event 7 in Table 2, respectively. Analyses of the proposed framework performance are presented in terms of PQ indices, cost, and load fulfillment and shedding.

5.2.1. PQ indices analysis

The performance of the proposed DSM-enabled OHPF framework for all sub-cases are presented in Figs. 8 to 10. Not all PQ indices are shown for all sub-cases. Only PQ indices under concern are presented for a corresponding sub-case. In Case 2a, for instance, VUF is displayed since it is the only PQ index with violation.

In general, the framework works effectively to avoid any PQ issues during the scheduling period. However, a few exceptions are noted. In Case 2a, during the interval $t \in [8, 12]$ there are 18 violations on VUF limit before the DSM application. When DSM Scheme 1 is applied, the number of violations is slightly reduced to 17. Notably, all 17 violations occur only in a single hour, that is at $t = 11$. This means that 17 out of 25 buses experience excessive VUF at this hour. Thus, in this case, DSM Scheme 1 is not very effective in suppressing VUF. The reason for this brief excessive VUF is that it is the most optimal loading configuration computed by the optimization algorithm despite giving a non-zero penalty function value. Consequently, the comparison between initial and DSM Scheme 1-supplemented cases should be carried out based on cost analysis, which is given in Section 5.2.2. Meanwhile, DSM Scheme 2 is able to omit all VUF limit violations during the scheduling period. This corresponds to 100% effectiveness. 100% effectiveness is

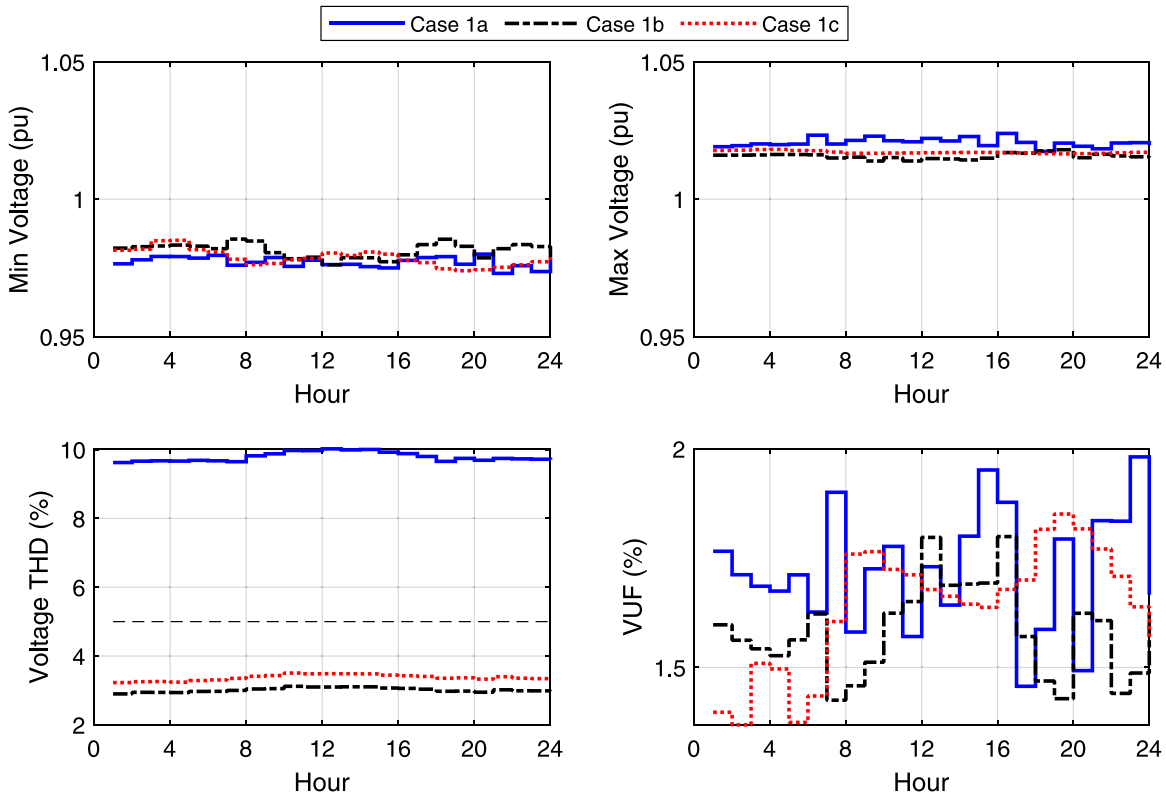

Fig. 7. Simulation results for Case 1.

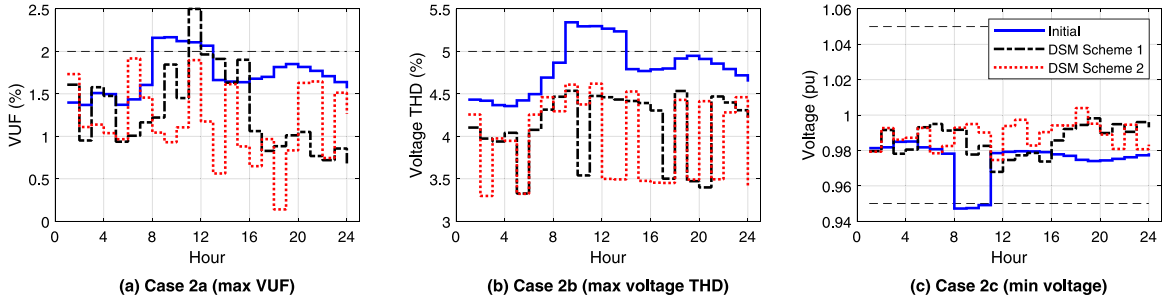

Fig. 8. PQ indices for single-disturbance sub-cases of Case 2.

also achieved by the proposed framework (for both DSM Scheme 1 and DSM Scheme 2) for Case 2b and Case 2c.

Fig. 9 shows the PQ performance for sub-cases involving violations on two PQ indices, while Fig. 10 shows that for Case 2 g, which is the only sub-case involving violations on three PQ indices. The general pattern is similar to those observed in Fig. 8. When dealing with the violations on voltage magnitude and voltage THD, the proposed framework performs greatly, achieving 100% effectiveness in avoiding such violations. This is applicable for DSM Scheme 1 and DSM Scheme 2. However, the performance of DSM Scheme 1 decreases when dealing with the VUF violation. As shown in Fig. 9(a.2), Fig. 9(c.2) and Fig. 10(c), the proposed framework fails to avoid excessive VUF values at $t = 11$, similar to that in Fig. 8. The DSM Scheme 1, at least, can reduce the duration of the excessive VUF values to only a single hour. Thus, at $t = 11$, DSM Scheme 1 is proposed not to be applied. Instead, DSM Scheme 2 should be utilized as a replacement at this point only.

5.2.2. Cost analysis

Fig. 11 presents the performance of the proposed DSM in terms of cost for all sub-cases. We do not display all cost components. Instead, we show only the total cost, DE cost (including startup cost and power production cost), grid exchange cost (equaling the revenue from exporting energy to the grid subtracted from the cost of exporting energy to the grid), and load shedding cost. From Fig. 11, we can see a common pattern that both DSM schemes are superior compared to the initial condition. Both DSM schemes can achieve total cost reductions but with different reduction levels. In Case 2a (Fig. 11(a)), Case 2b (Fig. 11(b)), and Case 2d (Fig. 11(d)), the reductions are relatively moderate. Meanwhile, we observe more significant reductions in Case 2c (Fig. 11(c)), Case 2e (Fig. 11(e)), Case 2f (Fig. 11(f)) and Case 2 g (Fig. 11(g)). This is related to the load shedding pattern associated with each sub-cases. Sub-cases involving voltage magnitude violations experience deeper load shedding, while the others encounter only moderate load shedding. It is noted that although load shedding cost is introduced when DSM is applied, the cost increase is compensated by more significant reductions in DE cost. This is the cost component that contributes significantly in the total cost reduction achieved by DSM.

Another reason behind the cost improvement attained by DSM is that we ignore the cost of ILT in this study. This is valid considering

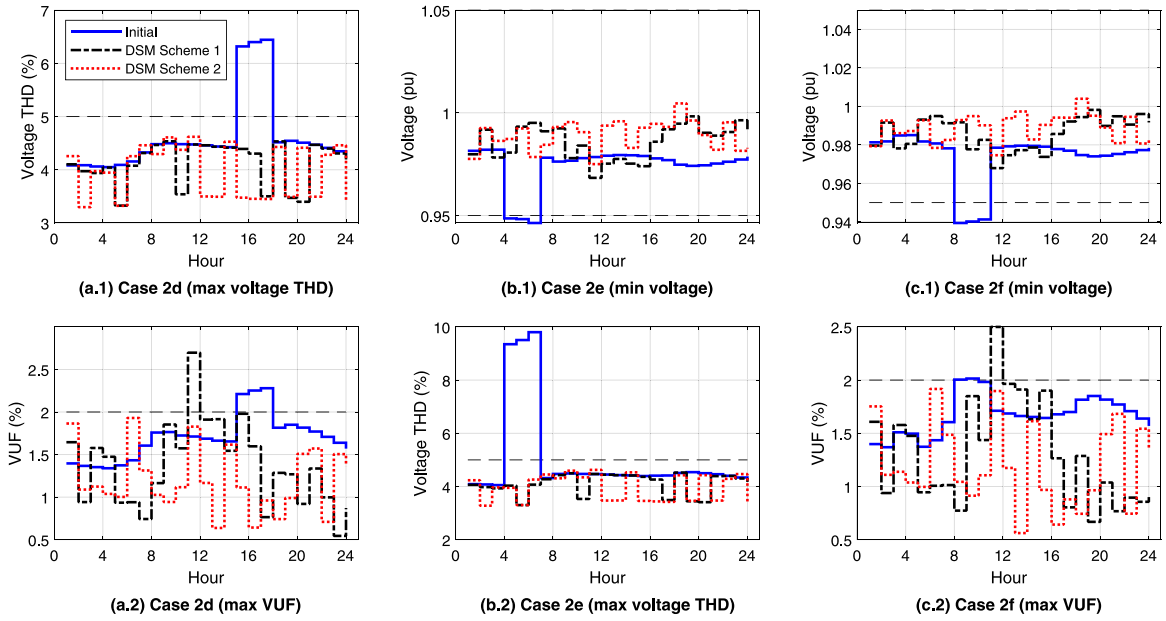

Fig. 9. PQ indices for double-disturbance sub-cases of Case 2.

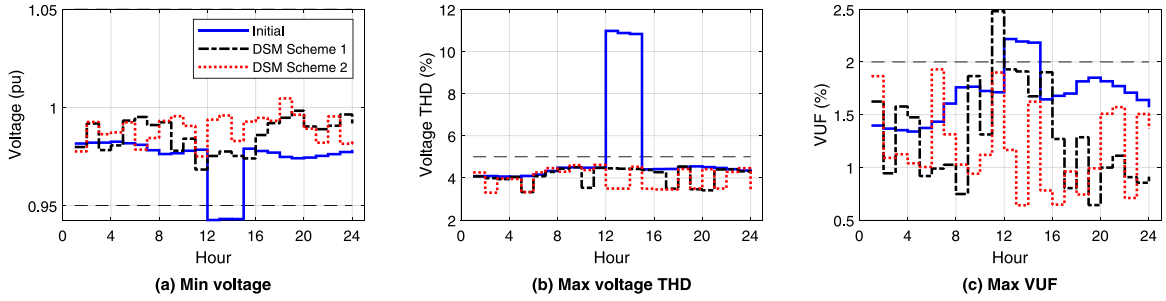

Fig. 10. PQ indices for triple-disturbance sub-case (Case 2 g).

a low-cost investment for realizing such a smart load transfer. Furthermore, we assume here that any dynamic voltage variations which take place in case of ILT are within acceptable region of the ITI curve [16]. Thus, it can be said in another way that load shedding cost itself is not enough to balance the decrease in DE cost.

When comparing DSM Scheme 1 and DSM Scheme 2, DSM Scheme 1 performs better in terms of the total cost. This is due to a higher shedding cost incurred by DSM Scheme 2. We can exploit this finding to remedy the failure of DSM Scheme 1 at $t = 11$ (see the corresponding explanation in Section 5.2.1), especially for Case 2a, Case 2d, Case 2f, and Case 2 g. It is therefore more effective to apply DSM Scheme 2 at $t = 11$, while letting the remaining hours with DSM Scheme 1. With this combination, an effectiveness of 100% can be achieved while the total cost is kept minimized.

5.2.3. *Load fulfillment and shedding analysis*

Load fulfillment analysis compares the actual total power supplied to all loads with their scheduled values. Significant differences between these two quantities mean significant load shedding, while moderate differences correspond to moderate load shedding. Fig. 12 shows the load fulfillment in all sub-cases. As can be seen, several differences are found especially in the time interval in which the PQ events take place. In Case 2a (Fig. 12(a)), for instance, significant differences are noted between $t = 8$ and $t = 12$ (as compared to other hours) because this is the interval of PQ event occurrence. This pattern is also applicable to other sub-cases. The most significant differences are noted in Case 2c (Fig. 12(c)), Case 2e (Fig. 12(e)), Case 2f (Fig. 12(f)), and Case 2 g (Fig. 12(g)). The reason is that, as described in Section 5.2.2, these are sub-cases in which violations on voltage magnitude limits are involved.

It is also noted at $t \in [16, 24]$ that the difference levels are also significant although no PQ events take place at this interval in most sub-cases. This is because the system scheduled load is high during this interval. The optimization algorithm opts not to fulfill this load perfectly. Therefore, load shedding is the best configuration for this interval.

Fig. 13 shows the load shedding patterns for all sub-cases more clearly. The load shedding in each hour is calculated as the sum of load shedding at all load buses. From Fig. 13, it is observed that load sheddings are applied in the hours where actions in Fig. 6 are carried out. However, the most significant load shedding are noted for sub-cases in which violations on voltage magnitude take place including Case 2c (Fig. 13(c)), Case 2e (Fig. 13(e)), Case 2f (Fig. 13(f)), and Case 2 g (Fig. 13(g)). This is because voltage magnitude is directly related to the load level. As the load jumps significantly when the violations occurs, the shedding follows accordingly. This also supplement the explanation in Section 5.2.2 that more significant cost reduction is related to more significant load shedding.

A special attention is given at $t = 18$ where sharp load shedding actions can be clearly seen. These high jumps are part of the best demand configuration resulting from the proposed OHPF. They are not related to a specific sub-case, thus can be seen at all sub-cases. Even in case the actions in Fig. 6 are absent, these jumps are still observed as long as DSM is applied.

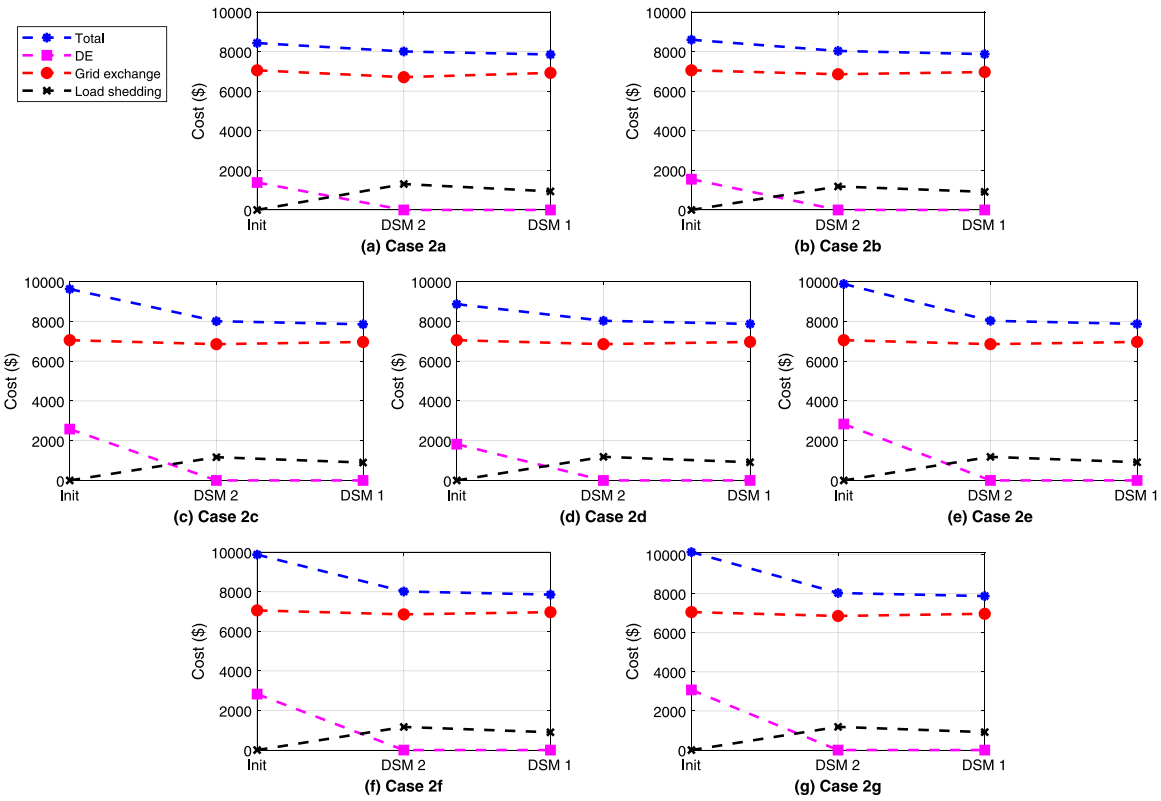

Fig. 11. Cost evaluation for Case 2.

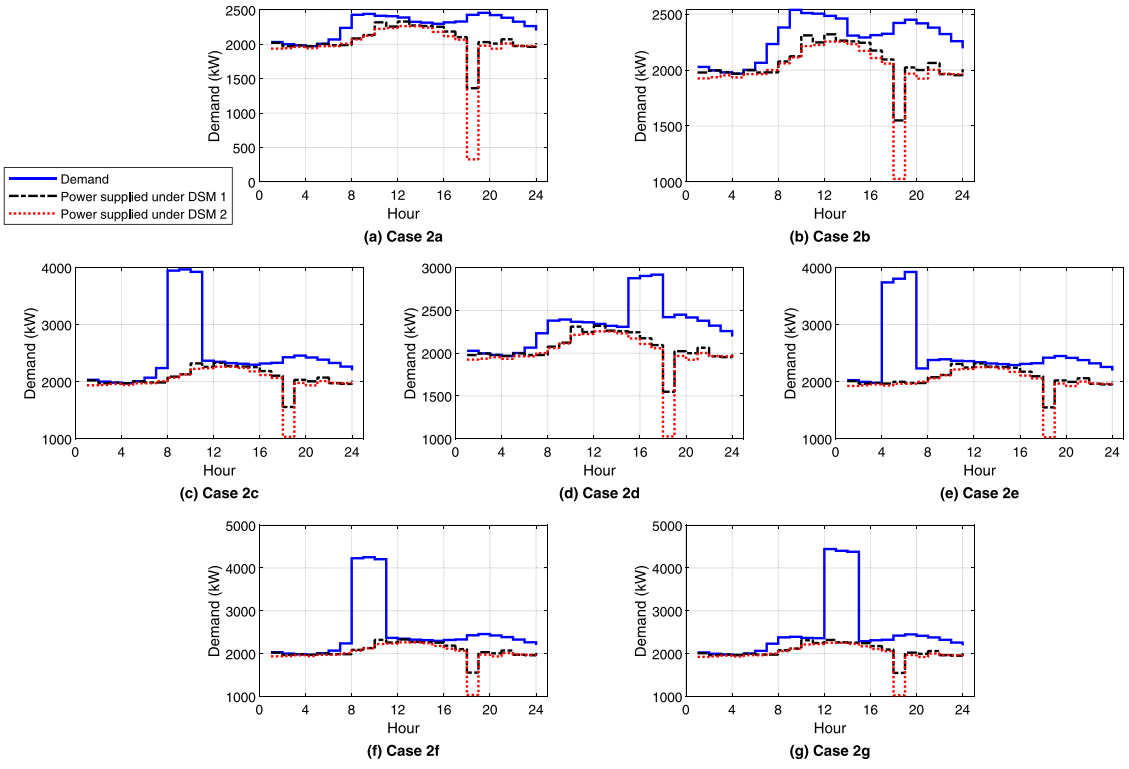

Fig. 12. Load fulfillment evaluation for Case 2.

5.3. Case 3

For Case 3, the intentional islanding operations are carried out only for OHPF with DSM Scheme 2. It is noted here that in Case 2 we find that the main grid supplies a significant portion of power to satisfy the load demand. Thus, the islanding operations cause significant load sheddings, which can only be accommodated by DSM Scheme 2.

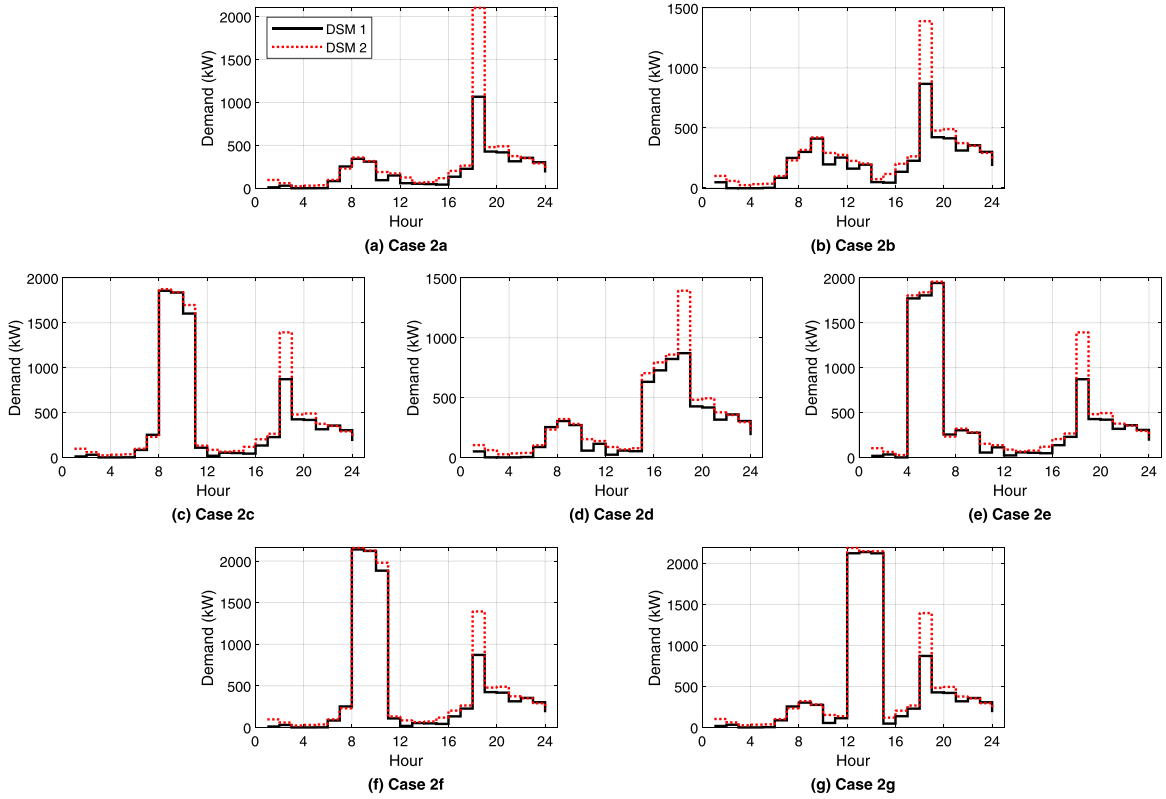

Fig. 13. Load shedding evaluation for Case 2.

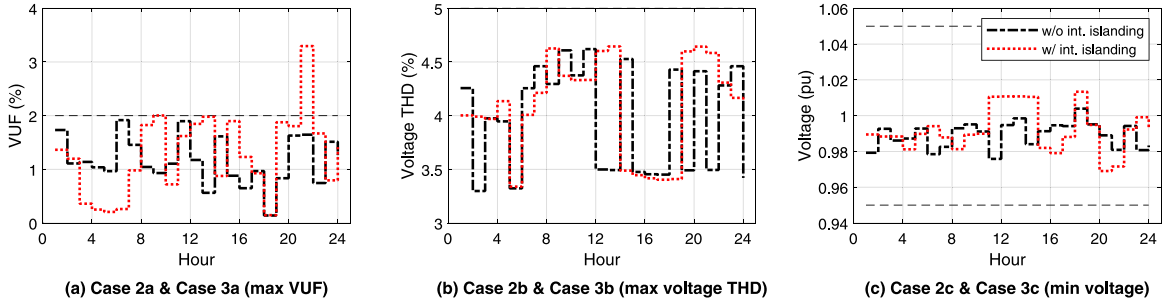

Fig. 14. PQ indices for single-disturbance sub-cases under DSM Scheme 2: Case 2 (w/o intentional islanding) & Case 3 (w/ intentional islanding).

In this section, we present the resulting PQ indices, the cost, and the load shedding patterns for Case 3.

5.3.1. PQ indices analysis

The PQ indices for single-disturbance, double-disturbance, and triple-disturbance sub-cases are presented in Fig. 14, Fig. 15, and Fig. 16, respectively. In general, islanding operations do not disturb the PQ indices value significantly, except for VUF values, in the sense that DSM Scheme 2 cannot fully suppress VUF to a permissible value. In Case 3a, VUF limit violation occurs at $t = 21$ (Fig. 14), while multiple violations are encountered at multiple hours in other sub-cases. This suggests that the intentional islanding should not be carried out, except when there is an urgent need to do so. For example, when a short circuit fault occurs in the main grid, an intentional islanding may be conducted to isolate the microgrid from the fault current.

5.3.2. Cost analysis

The total cost comparison between Case2 and Case 3 is presented in Table 8. As can be observed, the intentional islanding operations have increased the total operational cost for all sub-cases. The increases vary between $300 and $700, which can be deemed significant. The reason for this increase is obviously due to the increase in the load shedding cost due to more significant load shedding operations. The microgrid indeed stops purchasing energy from the main grid during the islanding period. However, for the given system data, the load shedding cost is too significant and exceeds the cost of purchasing energy from the main grid. This corresponds to a cost loss for the microgrid.

Table 8
Total cost comparison between Case 2 (w/o intentional islanding) & Case 3 (w/ intentional islanding).

Case	Total cost in each sub-case ($)						
	a	b	c	d	e	f	g
2	8006.47	8031.93	8012.28	8031.93	8031.69	8012.28	8031.93
3	8671.73	8411.07	8430.97	8136.02	8467.43	8364.28	8316.55

5.3.3. Load shedding analysis

The effect of the intentional islanding to the microgrid may be depicted more obviously by analyzing the load shedding pattern, which

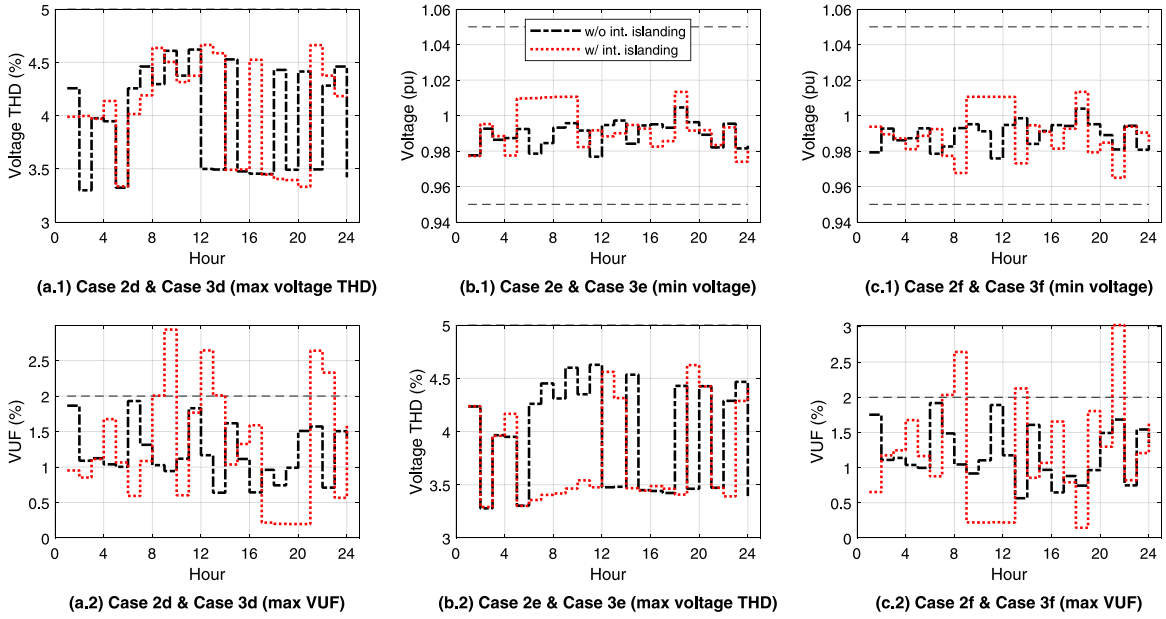

Fig. 15. PQ indices for double-disturbance sub-cases under DSM Scheme 2: Case 2 (w/o intentional islanding) & Case 3 (w/ intentional islanding).

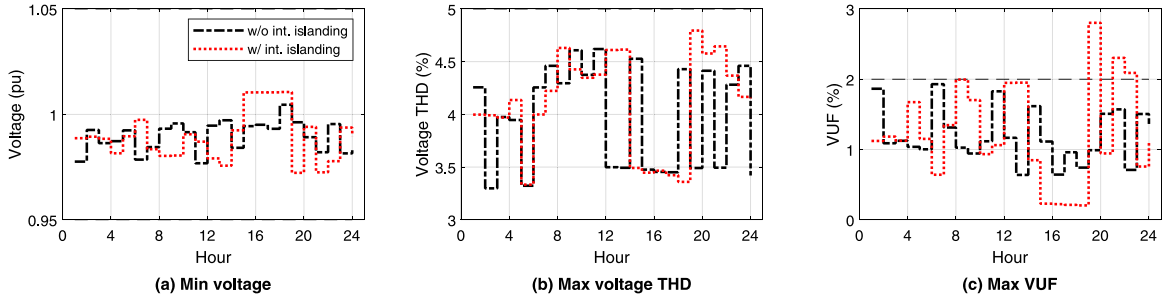

Fig. 16. PQ indices for triple-disturbance sub-case under DSM Scheme 2: Case 2 g (w/o intentional islanding) & Case 3 g (w/ intentional islanding).

is given in Fig. 17. In the first sub-case (Case 2a & Case 3a), the intentional islanding takes place from $t = 3$ to $t = 6$. The absence of incoming power from the main grid is consequently compensated by a significant load shedding at this interval. This is an example when the intentional islanding and load increase occur not at the same interval.

When the intentional islanding and load increase take place at the same time, the load shedding becomes greater and more significant. The examples for it is at Case 2e & Case 3e, which is shown in Fig. 17(e). The islanding occurs from $t = 5$ to $t = 9$, while the load increase occurs from $t = 4$ to $t = 6$. It means that the intersection takes place from $t = 5$ to $t = 6$. As a consequence, a huge load shedding should be carried out during this interval. The load shedding value with the islanding operation is approximately twice the load shed in the normal OHPF with DSM Scheme 2.

6. Conclusions

OHPF framework for a optimal scheduling of a grid-connected microgrid is proposed in this paper. Within this framework, DSM-based mechanism is also constructed to avoid PQ disturbances. This mechanism is integrated into the optimization part of OHPF as a set of load constraints and is divided into two schemes, namely DSM Scheme 1 and Scheme 2, which are different on the level of tightness in limiting the loading adjustment. To assess the effectiveness of the proposed framework, it is tested using the modified IEEE 37-bus feeder against different PQ events employing three PQ indices under both normal and intentional islanding conditions. The following points can be concluded.

1. Under normal condition, both DSM schemes perform effectively to avoid any PQ disturbance. While DSM Scheme 2 can achieve 100% effectiveness, DSM Scheme 2 leaves a flaw at $t = 11$ where it fails to suppress the maximum VUF value below the limit. Thus, in case of events with VUF limit violation, DSM Scheme 1 is still preferred (due to a lower total cost) except at $t = 11$, which should be tackled by DSM Scheme 2.
2. Under the presence of intentional islanding, only DSM Scheme 2 can be used because of the greater load shedding requirement. DSM Scheme 2 stil performs well, but cannot attain 100% effectiveness. Intentional islanding also increases the total cost. Therefore, it is not recommended to perform intentional islanding unless there is an urgent need.
3. In addition to avoiding PQ disturbances, the scheduling employing both DSM schemes achieves lower total costs as compared to that of the initial case, i.e., the case without DSM. This is possible due to significant reductions in DE cost when DSM is applied. Thus, the load shedding cost incurred by DSM is compensated by DE cost reduction.
4. In terms of load shedding performed by DSM, the most significant shedding is observed when the voltage magnitude limit is

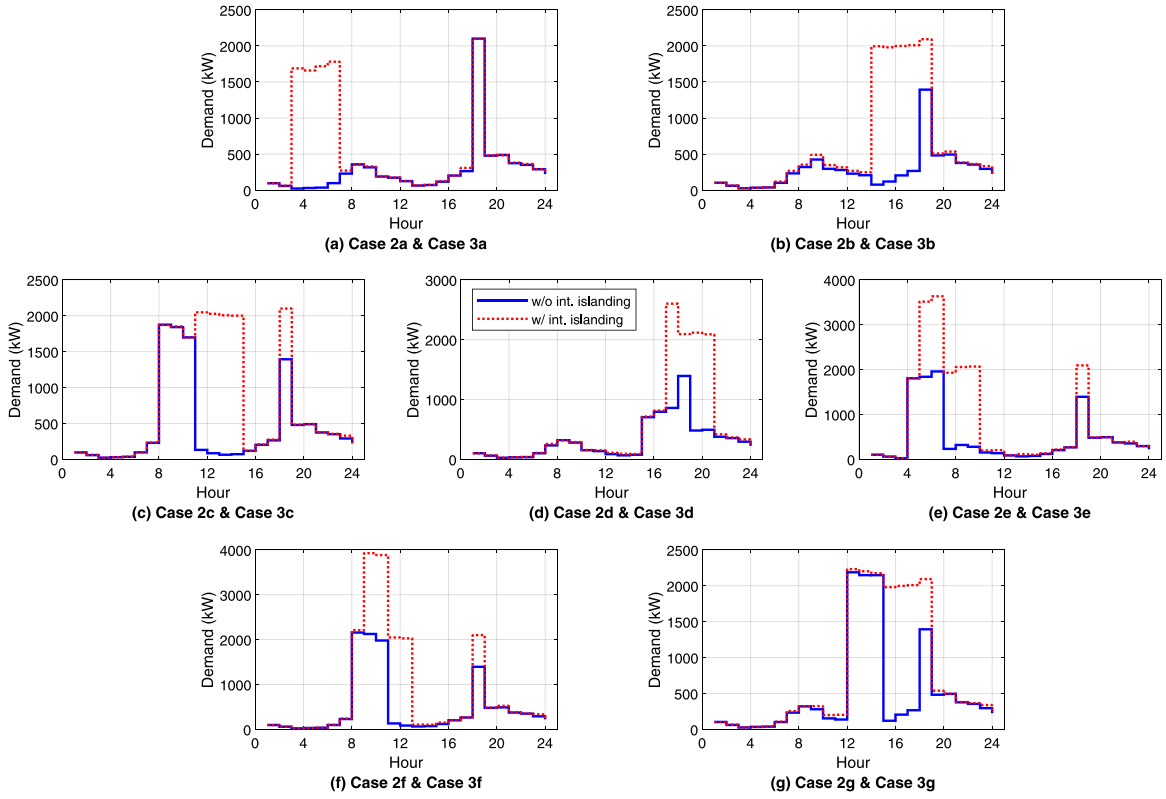

Fig. 17. The pattern of load shedding under DSM Scheme 2: Case 2 (w/o intentional islanding) & Case 3 (w/ intentional islanding).

violated. This is due to the fact that voltage magnitude is directly related to the demand level.

For further studies, the uncertainties in WT and PV power output will be considered in the scheduling algorithm. Furthermore, additional PQ indices such as individual harmonic distortion (IHD) and RMS current are also to be included.

CRediT authorship contribution statement

Firmansyah Nur Budiman: Conceptualization, Methodology, Software, Formal analysis, Writing – original draft. **Makbul A.M. Ramli:** Supervision, Validation, Writing – reviewing & editing, Funding acquisition. **Houssem R.E.H. Bouchekara:** Validation, Writing – review & editing. **Ahmad H. Milyani:** Software, Validation, Resources.

Declaration of competing interest

The authors declare that they have no known competing financial interests or personal relationships that could have appeared to influence the work reported in this paper.

Data availability

Data will be made available on request.

Acknowledgments

The authors extend their appreciation to the Deputyship for Research and Innovation, Ministry of Education in Saudi Arabia for funding this research work through the project number IFPHI-104-135-2020 and King Abdulaziz University, DSR, Jeddah, Saudi Arabia.

References

[1] Thirunavukkarasu GS, Seyedmahmoudian M, Jamei E, Horan B, Mekhilef S, Stojcevski A. Role of optimization techniques in microgrid energy management systems—A review. Energy Strategy Rev 2022;43:100899. http://dx.doi.org/10.1016/J.ESR.2022.100899.

[2] Alizadeh A, Kamwa I, Moeini A, Mohseni-Bonab SM. Energy management in microgrids using transactive energy control concept under high penetration of renewables; A survey and case study. Renew Sustain Energy Rev 2023;176:113161. http://dx.doi.org/10.1016/J.RSER.2023.113161.

[3] Khan I, Vijay AS, Doolla S. Nonlinear load harmonic mitigation strategies in microgrids: State of the art. IEEE Syst J 2022;16(3):4243–55. http://dx.doi.org/10.1109/JSYST.2021.3130612.

[4] Nejabatkhah F, Li YW, Tian H. Power quality control of smart hybrid AC/DC microgrids: An overview. IEEE Access 2019;7:52295–318. http://dx.doi.org/10.1109/ACCESS.2019.2912376.

[5] Shahzad S, Abbasi MA, Chaudhry MA, Hussain MM. Model predictive control strategies in microgrids: A concise revisit. IEEE Access 2022;10:122211–25. http://dx.doi.org/10.1109/ACCESS.2022.3223298.

[6] Jumani TA, Mustafa MW, Alghamdi AS, Rasid MM, Alamgir A, Awan AB. Swarm intelligence-based optimization techniques for dynamic response and power quality enhancement of AC microgrids: A comprehensive review. IEEE Access 2020;8:75986–6001. http://dx.doi.org/10.1109/ACCESS.2020.2989133.

[7] Miah MS, Hossain Lipu MS, Ansari S, Meraj ST, Hasan K, Masaoud A, et al. Energy storage controllers and optimization schemes integration to microgrid: An analytical assessment towards future perspectives. IEEE Access 2022;10:52982–3014. http://dx.doi.org/10.1109/ACCESS.2022.3174123.

[8] Elkholy MM, El-Hameed MA, El-Fergany AA. Harmonic analysis of hybrid renewable microgrids comprising optimal design of passive filters and uncertainties. Electr Power Syst Res 2018;163:491–501. http://dx.doi.org/10.1016/j.epsr.2018.07.023.

[9] Doyran RV, Sedighizadeh M, Rezazadeh A, Alavi SMM. Optimal allocation of passive filters and inverter based DGs joint with optimal feeder reconfiguration to improve power quality in a harmonic polluted microgrid. Renew Energy Focus 2020;32:63–78. http://dx.doi.org/10.1016/J.REF.2019.12.001.

[10] Pramila V, Chandramohan S. Intelligent energy scheduling in a microgrid with custom power devices. Int J Electr Eng Educ 2020;58(2):572–89. http://dx.doi.org/10.1177/0020720920929661.

[11] Micallef A, Apap M, Spiteri-Staines C, Guerrero JM. Mitigation of harmonics in grid-connected and islanded microgrids via virtual admittances and impedances. IEEE Trans Smart Grid 2017;8(2):651–61. http://dx.doi.org/10.1109/TSG.2015.2497409.

[12] Gothner F, Roldan Perez J, Torres R, Midtgard OM. Harmonic virtual impedance design for optimal management of power quality in microgrids. IEEE Trans Power Electron 2021;36(9):10114–26. http://dx.doi.org/10.1109/TPEL.2021.3065755.

[13] Elmetwaly AH, Eldesouky AA, Sallam AA. An adaptive D-FACTS for power quality enhancement in an isolated microgrid. IEEE Access 2020;8:57923–42. http://dx.doi.org/10.1109/ACCESS.2020.2981444.

[14] Liu J, Miura Y, Ise T. Cost-function-based microgrid decentralized control of unbalance and harmonics for simultaneous bus voltage compensation and current sharing. IEEE Trans Power Electron 2019;34(8):7397–410. http://dx.doi.org/10.1109/TPEL.2018.2879340.

[15] Babu NP, Guerrero JM, Siano P, Peesapati R, Panda G. An improved adaptive control strategy in grid-tied PV system with active power filter for power quality enhancement. IEEE Syst J 2021;15(2):2859–70. http://dx.doi.org/10.1109/JSYST.2020.2985164.

[16] Shahnia F, Wolfs PJ, Ghosh A. Voltage unbalance reduction in low voltage feeders by dynamic switching of residential customers among three phases. IEEE Trans Smart Grid 2014;5(3):1318–27. http://dx.doi.org/10.1109/TSG.2014.2305752.

[17] Thomas D, D'Hoop G, Deblecker O, Genikomsakis KN, Ioakimidis CS. An integrated tool for optimal energy scheduling and power quality improvement of a microgrid under multiple demand response schemes. Appl Energy 2020;260:114314. http://dx.doi.org/10.1016/J.APENERGY.2019.114314.

[18] Erenoğlu AK, Şengör I, Erdinç O, Taşcıkaraoğlu A, Catalão JP. Optimal energy management system for microgrids considering energy storage, demand response and renewable power generation. Int J Electr Power Energy Syst 2022;136:107714. http://dx.doi.org/10.1016/J.IJEPES.2021.107714.

[19] Nourollahi R, Salyani P, Zare K, Mohammadi-Ivatloo B. Resiliency-oriented optimal scheduling of microgrids in the presence of demand response programs using a hybrid stochastic-robust optimization approach. Int J Electr Power Energy Syst 2021;128:106723. http://dx.doi.org/10.1016/J.IJEPES.2020.106723.

[20] Tan Y, Cao Y, Li Y, Lee KY, Jiang L, Li S. Optimal day-ahead operation considering power quality for active distribution networks. IEEE Trans Autom Sci Eng 2017;14(2):425–36. http://dx.doi.org/10.1109/TASE.2016.2629477.

[21] Geth F, Van Acker T. Harmonic optimal power flow with transformer excitation. Electr Power Syst Res 2022;213:108604. http://dx.doi.org/10.1016/J.EPSR.2022.108604.

[22] Youssef KH. Power quality constrained optimal management of unbalanced smart microgrids during scheduled multiple transitions between grid-connected and islanded modes. IEEE Trans Smart Grid 2017;8(1):457–64. http://dx.doi.org/10.1109/TSG.2016.2577643.

[23] Çiçek A, Erenoğlu AK, Erdinç O, Bozkurt A, Taşcıkaraoğlu A, Catalão JP. Implementing a demand side management strategy for harmonics mitigation in a smart home using real measurements of household appliances. Int J Electr Power Energy Syst 2021;125:106528. http://dx.doi.org/10.1016/J.IJEPES.2020.106528.

[24] Silva JAA, López JC, Guzman CP, Arias NB, Rider MJ, da Silva LC. An IoT-based energy management system for AC microgrids with grid and security constraints. Appl Energy 2023;337:120904. http://dx.doi.org/10.1016/J.APENERGY.2023.120904.

[25] Bajaj M, Singh AK, Alowaidi M, Sharma NK, Sharma SK, Mishra S. Power quality assessment of distorted distribution networks incorporating renewable distributed generation systems based on the analytic hierarchy process. IEEE Access 2020;8:145713–37. http://dx.doi.org/10.1109/ACCESS.2020.3014288.

[26] Meng L, Guerrero JM. Optimization for customized power quality service in multibus microgrids. IEEE Trans Ind Electron 2017;64(11):8767–77. http://dx.doi.org/10.1109/TIE.2017.2701767.

[27] Prabawa P, Choi DH. Hierarchical volt-VAR optimization framework considering voltage control of smart electric vehicle charging stations under uncertainty. IEEE Access 2021;9:123398–413. http://dx.doi.org/10.1109/ACCESS.2021.3109621.

[28] Luo S, Peng K, Hu C, Ding SX, Fan H. A residual-generator-based plug-and-play control scheme toward enhancing power quality in AC microgrids. IEEE Trans Ind Electron 2022;69(8):8146–56. http://dx.doi.org/10.1109/TIE.2021.3104602.

[29] Keypour R, Adineh B, Khooban MH, Blaabjerg F. A new population-based optimization method for online minimization of voltage harmonics in islanded microgrids. IEEE Trans Circuits Syst II 2020;67(6):1084–8. http://dx.doi.org/10.1109/TCSII.2019.2927208.

[30] dos Santos Alonso AM, Brandao DI, Caldognetto T, Marafão FP, Mattavelli P. A selective harmonic compensation and power control approach exploiting distributed electronic converters in microgrids. Int J Electr Power Energy Syst 2020;115:105452. http://dx.doi.org/10.1016/J.IJEPES.2019.105452.

[31] Chishti F, Murshid S, Singh B. Development of wind and solar based AC microgrid with power quality improvement for local nonlinear load using MLMS. IEEE Trans Ind Appl 2019;55(6):7134–45. http://dx.doi.org/10.1109/TIA.2019.2923575.

[32] Alshehri J, Khalid M. Power quality improvement in microgrids under critical disturbances using an intelligent decoupled control strategy based on battery energy storage system. IEEE Access 2019;7:147314–26. http://dx.doi.org/10.1109/ACCESS.2019.2946265.

[33] Hou X, Sun K, Zhang N, Teng F, Zhang X, Green T. Priority-driven self-optimizing power control scheme for interlinking converters of hybrid AC/DC microgrid clusters in decentralized manner. IEEE Trans Power Electron 2022;37(5):5970–83. http://dx.doi.org/10.1109/TPEL.2021.3130112.

[34] Brandao DI, Ferreira WM, Alonso AM, Tedeschi E, Marafao FP. Optimal multiobjective control of low-voltage AC microgrids: Power flow regulation and compensation of reactive power and unbalance. IEEE Trans Smart Grid 2020;11(2):1239–52. http://dx.doi.org/10.1109/TSG.2019.2933790.

[35] Su W, Wang J, Roh J. Stochastic energy scheduling in microgrids with intermittent renewable energy resources. IEEE Trans Smart Grid 2014;5(4):1876–83. http://dx.doi.org/10.1109/TSG.2013.2280645.

[36] Electric Power Research Institute. Simulation tool – opendss. 2023, URL https://smartgrid.epri.com/SimulationTool.aspx.

[37] Budiman FN, Ramli MA, Milyani AH, Bouchekara HR, Rawa M, Muktiadji RF, et al. Stochastic optimization for the scheduling of a grid-connected microgrid with a hybrid energy storage system considering multiple uncertainties. Energy Rep 2022;8:7444–56. http://dx.doi.org/10.1016/J.EGYR.2022.05.249.

[38] D'Hoop G, Deblecker O, Thomas D. Power quality improvement of a microgrid with a demand-side-based energy management system. In: Ghofrani M, editor. Micro-grids - applications, operation, control and protection. London, UK: IntechOpen; 2019, p. 1–24. http://dx.doi.org/10.5772/INTECHOPEN.83604.

[39] IEEE. 1159-2019 - IEEE recommended practice for monitoring electric power quality. 2019.

[40] Dunning I, Huchette J, Lubin M. JuMP: A modeling language for mathematical optimization. SIAM Rev 2017;59(2):295–320. http://dx.doi.org/10.1137/15M1020575, arXiv:1508.01982.

[41] Gurobi Optimization LLC. Gurobi optimizer reference manual. 2023, URL https://www.gurobi.com.

[42] Resources – IEEE PES test feeder. 2023, URL https://cmte.ieee.org/pes-testfeeders/resources/.

[43] Masoum MA, Moses PS, Deilami S. Load management in smart grids considering harmonic distortion and transformer derating. In: Innovative smart grid technologies conference. Gaithersburg, MD, USA: IEEE; 2010, p. 1–6. http://dx.doi.org/10.1109/ISGT.2010.5434738.

[44] Staats PT, Grady WM, Arapostathis A, Thallam RS. A statistical method for predicting the net harmonic currents generated by a concentration of electric vehicle battery chargers. IEEE Trans Power Deliv 1997;12(3):1266. http://dx.doi.org/10.1109/61.637002.

[45] Midcontinent Independent System Operator. MISO real-time operations displays. 2022, URL https://www.misoenergy.org/markets-and-operations/real-time--market-data/operations-displays/.

[46] Abbas AS, El-Sehiemy RA, Abou El-Ela A, Ali ES, Mahmoud K, Lehtonen M, et al. Optimal harmonic mitigation in distribution systems with inverter based distributed generation. Appl Sci 2021;11(2):774. http://dx.doi.org/10.3390/APP11020774.